FINAL REPORT

KU-BAND RENDEZVOUS RADAR PERFORMANCE COMPUTER SIMULATION MODEL

CONTRACT NO. NAS9-15840

JUNE 1984

Prepared by:
Radar Systems Group
Hughes Aircraft Company
2000 E. Imperial Highway
El Segundo, California 90245

Prepared for:
National Aeronautics and Space Administration
Johnson Space Flight Center
Houston, Texas 77058
J. W. Griffin, Technical Officer

RSG P&G NO. P40629

KU-BAND RENDEZVOUS RADAR PERFORMANCE COMPUTER SIMULATION MODEL

FINAL REPORT

June, 1984

CONTRACT NO. NAS 9-15840

Prepared for: National Aeronautics and Space Administration
Lyndon B. Johnson Space Center
Houston, Texas 77058
J.W. Griffin, Technical Monitor

Prepared by: H.G. Magnusson and M.F. Goff
Systems Engineering Department
Advanced Programs Division
Radar Systems Group
Hughes Aircraft Company
El Segundo, CA 90245

CONTENTS

Page intentionally left blank

Page intentionally left blank

LIST OF ILLUSTRATIONS

LIST OF ILLUSTRATIONS (Continued)

LIST OF TABLES

LIST OF TABLES (Continued)

LIST OF TABLES (Continued)

1. INTRODUCTION AND SUMMARY

This report summarizes and documents all work performed on the Ku-Band Rendezvous Radar Performance Computer Simulation Model program since the release of the preliminary final report on 31 July 1980. Its submittal is to fulfill the Data Requirement List (DRL) Number T-1544, Item Number 2 under NASA Contract NAS9-15840.

Developments on the program since July 1980 fall into three distinct categories: (1) modifications to the existing Ku-band radar tracking performance computer model, (2) the addition of a highly accurate, nonreal-time search and acquisition performance computer model to the total software package developed on this program, and (3) development of radar cross section (RCS) computation models for three additional satellites. All changes in the tracking model involved improvements in the automatic gain control (AGC) and the radar signal strength (RSS) computer models. Although the search and acquisition computer models were developed under the auspices of the Hughes Aircraft Company Ku-Band Integrated Radar and Communications Subsystem program office, they have been supplied to NASA as part of the Ku-band radar performance computer model package. Their purpose is to predict Ku-band acquisition performance for specific satellite targets on specific missions. RCS models were developed for three satellites: the Long Duration Exposure Facility (LDEF) spacecraft, the Solar Maximum Mission (SMM) spacecraft, and the Space Telescope.

The remainder of the report is structured as follows. Section 2 provides the details of all improvements to the original track simulation model. This includes the addition of a more accurate AGC model, an A/D quantization noise model, and a more accurate RSS model. Section 3 provides a summary description of the new search and acquisition performance prediction package. This description includes all changes which were made as a result of the System

Design Verification Tests (SDVT) performed at the Baldwin Hills test facility. Section 4 provides the details of the various spacecraft RCS computer models. Finally, listings of the most recent version of all computer programs will be supplied in the appendix to this report.

2. TRACK MODEL MODIFICATIONS

The extent of the track model modifications since July 1980 was the addition of two new modules (one to compute accurate effects of system AGC and one to inject the effects of A/D converter saturation) and an upgrade in the fidelity of the radar signal strength (RSS) module. Details of these models are provided in this section.

2.1 AGC MODEL DESCRIPTION

In the version of the Ku-band radar track model published in the preliminary report, the AGC was assumed to act instantaneously to hold the signal to the desired attack point at the A/D input. Furthermore, the effects of A/D quantization noise were ignored. The effect of this model simplification was to produce unlimited tracking accuracy as the signal-to-noise power ratio (SNR) continued to increase. Thus, under large signal conditions, all tracking error estimates were too optimistic. With the inclusion of the AGC model described herein, the track simulation now provides accurate estimates of the AGC response from data cycle to data cycle. It includes the following features:

1. The AGC increment for the next data cycle is determined by subtracting the mean signal level at the log converter output from a prestored value which represents a signal power of $4q^2$ at the A/D input,

2. It includes the effects of quantization noise injected by the A/D converter,

3. It allows a maximum of 10 dB increment in AGC or a minimum of -10 dB decrement in AGC per data cycle,

4. The absolute AGC value cannot drop below 6 dB, the nominal search AGC value.

A crude A/D converter saturation model has been implemented in conjunction with this model to increase AGC response fidelity in anticipation of large, sudden increases in satellite RCS values.

The AGC algorithm can be summarized as follows:

Step 1: Compute the AGC change, ΔAGC, based on the present mean signal level estimate at the log converter output.

Step 2: If $\Delta AGC \geq 10$ dB, then $\Delta AGC = 10$ dB, or if $\Delta AGC \leq -10$ dB, then $\Delta AGC = -10$ dB.

Step 3: Compute the new AGC.

Step 4: If new AGC ≤ 6 dB, then new AGC = 6 dB.

Actual implementation of the AGC model is done as follows:

$$AGC(N+1) = AGC(N) \cdot AGCERR(N) \qquad (2\text{-}1)$$

where $AGCERR(N) = k_1 G/(AGC(N)(SNR_{DT}(N)+1) + k_2)$

G = Signal-to-noise power ratio (SNR) gain from the A/D output to the doppler filter output,

SNR_{DT} = Signal-to-thermal noise power ratio at the doppler filter output,

$k_1 = (2q)^2/N_T$,

$k_2 = (q)^2/(12N_T)$,

N_T = unAGC'd thermal noise power at the A/D input.

k_1 can be interpreted as the ratio of the desired AGC'd track signal power level at the A/D input to the unAGC'd thermal noise power level at the A/D input, k_2 is interpreted as the ratio of the quantization noise power, $q^2/12$, to the unAGC'd thermal noise power at the A/D input. Finally, in order to be consistent with the present code, we will set $G = 4\ P_s$. The values for k_1, k_2, G and P_s for the various modes and range intervals are summarized in Table 2-1.

TABLE 2-1. AGC CALCULATION CONSTANTS

Range Interval, Ft.	N ,q	k	k	G	P
Passive					
<2560	156.4	0.0256	0.00053	16	4
(2560,5750)	7.84	0.51	0.011	16	4
(5760,11510)	7.84	0.51	0.011	8	2
(11510,23030)	7.84	0.51	0.011	16	4
(23040,43510)	7.84	0.51	0.011	32	16
>43510	7.84	0.51	0.011	64	32
Active					
<49910	156.4	0.0256	0.00053	16	4
>49920	7.84	0.51	0.011	8	2

Some comments on the accuracy of this algorithm versus actual AGC operation are in order. We first note that the form for predicting the AGC change given in Equation 2-1 is quite accurate. (A derivation of this equation is provided in Appendix A of this volume.) It has the A/D quantization noise and the noise floor concept folded into the calculation. As noted earlier, the quantization noise includes only the contribution from the A/D converter and is assumed to have a power of $q^2/12$ where q represents the voltage of a single A/D step. All other quantization noise sources are dwarfed in comparison to this source, especially when comparing their relative effects at the doppler filter output. The search thermal noise AGC value or the "noise floor" in this expression is fixed at 6 dB. This floor represents the search AGC value at the time the target is detected. In reality, this number is a random process, fluctuating from acquisition to acquisition. However, we treat the noise floor as a deterministic value and assign it a value equal to the mean of the random process, i.e., 6 dB for all acquisitions.

2.2 A/D SATURATION MODEL DESCRIPTION

A simple model for injecting A/D saturation effects into the tracking signal response was developed in anticipation of encountering sudden, large increases in receive signal strength when rendezvousing with various satellite targets. The model is fairly crude and is based on the concept that the total signal-plus-noise power at the A/D output should be limited to $(7q)^2$. In algorithmic form this can be expressed as

Step 1: Compute the signal-plus-noise power at the A/D input.

Step 2: If the total power is greater than $(7q)^2$, then limit this power to $(7q)$.

In the implementation of this algorithm, the total signal-plus-noise power at the A/D input is computed using the expression,

$$\text{Total Power} = AGC(N)N_T(SNR_{DT}(N)/G+1) \qquad (2\text{-}2)$$

where SNR_{DT}/G is equivalent to SNR_{VT}, the signal-to-thermal noise power ratio at the A/D input. SNR_{VT} is represented in this form because it is not easy to compute directly within the simulation, while SNR_{DT} and G are easily accessed. Hence, the indirect form of the calculation is used.

2.3 RSS MODEL MODIFICATION

In the original model submitted with the preliminary final report, the radar signal strength was set equal to the SNR at the video filter output. That is,

$$RSS(dB) = 10 \log(SNR_{VT}) \qquad (2\text{-}3)$$

This is a reasonable approximation to the actual system RSS estimator for most signal strengths of interest. However, since the EA-2 actually generates the RSS value using its own AGC estimate and since an AGC algorithm is now

implemented in the simulation, it was decided to implement the exact RSS calculation algorithm from the EA-2. This algorithm can be expressed as

$$RSS(N) = 10 \log(1/AGC(N)) - 6 \qquad (2\text{-}4)$$

where AGC(N) is computed using Equation 2-1. It should be noted at this point that this RSS estimate is highly accurate for all ranges greater than 640 feet. Inside 640 feet, however, there are particular conditions when this value will be 40 dB too high. The reason for this error is not the form of the algorithm in Equation 2-4, but in the AGC(N) calculation. The EA-2 AGC algorithm ignores the fact that TWT bypass has been commanded under certain conditions, producing a 40-dB error. The AGC algorithm used in the simulation does not have this anomaly modeled. For further details on this particular anomaly, one can consult the system signature log [2].

Before leaving this section, it would be instructive to point out the differences between the original RSS model of Equation 2-3 and the present model given in Equation 2-4. Now, ideally, one would like to have an RSS which is exactly equal to the SNR . However, what the actual algorithm gives can be seen by rewriting Equation 2-4 in the equivalent form

$$RSS = 10 \log[SNR_{VT} + 1/G] + 10 \log[N_T/(4q^2 - q^2/12G)] - 6 \qquad (2\text{-}5)$$

or, using the fact that $4q^2 >> q^2/12G$,

$$RSS = 10 \log[SNR_{VT} + 1/G] + 10 \log[N_T/4q^2] - 6 \qquad (2\text{-}6)$$

From this form of the equation one can see that there is a bias in the signal strength estimate at all ranges. Additional probing has shown this bias to be produced by the use of different AGC attack points in search and track, i.e., a 1.4 q-level attack point is used in search, and a 2q-level attack point is used in track. However, neglecting the bias in Equation 2-6, one can see that RSS is equal to SNR_{VT} in dB since 1/G is small compared to SNR_{VT} for most ranges of interest. For further information on RSS, one can consult several papers (References [3] to [5]) dealing with various aspects of the RSS computation.

3. SEARCH AND ACQUISITION PERFORMANCE MODEL COMPUTER SOFTWARE PACKAGE

This section provides a brief description of the search and acquisition performance model computer software package. The package was supplied to NASA under the present contract for the purpose of accurately predicting Ku-band radar acquisition performance against specific targets on specific missions. First, a brief description of model evolution is provided to give the reader a feeling for the overall fidelity and accuracy of the computer model. Next, the structure of the package is summarized. And, finally, details of the major components of the package are presented.

3.1 BACKGROUND

The search and acquisition performance models were originally developed as part of a massive effort directed by the Hughes Aircraft Company Ku-Band Integrated Radar and Communications Subsystem program office to evaluate and surface possible problems in the radar target acquisition process prior to system integration and testing. When the program moved into the system design verification testing, computer model results were cross checked against system test results at several points, covering the boundaries of the specified performance envelope. Results of the cross check can be summarized as follows. Computer model data and the test results were found to be in good agreement in the weak signal cases. However, in the large signal cases the computer model results were far too optimistic compared to the test results. Also, additional probing of the large signal case revealed that some of the failure mechanisms found in system test data were absent in the computer model data. Once the failure mechanisms in the large signal test data were thoroughly understood, a two prong attack on the problem was initiated. Along one path, system fixes were determined which would enhance acquisition performance and

simultaneously along a separate path, several fidelity improvements were made in the computer model so that it could be used to evaluate the recommended hardware changes. Results of these two activities were that the upgraded computer model predicted the proposed hardware fixes should make a spectacular improvement in target acquisition performance. In the final phase of system design verification testing, these computer predictions were corroborated across the entire performance envelope.

3.2 SOFTWARE PACKAGE STRUCTURE

The search and acquisition software package consists of five separate, self-contained computer models. Each of these models is used to predict acquisition performance for different radar modes or different range intervals within a mode as shown in Table 3-1. While all five models have the same general construction, some significant differences within the signal processing and AGC modules will be found among the various models. In fact, the primary driving forces in the division of the acquisition models among the modes and range intervals were the differences in the detectors, range gate configurations, and the AGC logic. For example, GPC-ACQ short range (range less than 2560 feet) employs a single pulse, fixed threshold detector, a 16 doppler filter CFAR detector, and additional special AGC logic. On the other hand, GPC-ACQ long range (ranges greater than 43520 feet) uses a 32 doppler filter CFAR detector and a 16 doppler filter CFAR detector, but does not have the additional special AGC logic.

TABLE 3-1. SUMMARY OF INDIVIDUAL ACQUISITION MODELS

Radar Mode	Range Interval, Feet
GPC-ACQ, Passive	<2560
GPC-ACQ, Passive	(2560, 43510)
GPC-ACQ, Passive	>43510
Auto, Passive	All ranges
Active	All ranges

A detailed description of the general construction of these models is provided in Reference [6]. In the remainder of Section 3, brief descriptions of each of the five models will be provided with the emphasis placed on the sequence of signal processing that transitions the radar from search to track.

3.3 GPC-ACQ, PASSIVE MODELS

As noted in Table 3-1, GPC-ACQ, passive mode is broken into three separate computer models. The division is based onthe signal processing differences found in the various range intervals. One model, termed the "short range model," covers the interval (100 feet, 2550 feet) and predicts performance for all high sample rate, 7 kHz PRF cases. A second model, called the "medium range model," covers the interval (2560 feet, 43510 feet) and provides performance predictions for all low sample rate, 7 kHz PRF applications. And, the third model, known as the "long range model," covers all ranges greater than 43510 feet, giving acquisition performance predictions for all low sample rate, 3 kHz PRF applications.

Figure 3-1, taken from Reference [7], summarizes the search and acquisition logic for all three range intervals. (Note that this flow diagram provides the search and acquisition logic for the GPC-DES mode as well by simply following the nonscanning paths.) While this diagram provides a fair amount of detail, it is felt that it would be useful to provide additional information on the signal processing for several of the basic acquisition sequences. We first note that there is probably an infinite number of possible acquisition sequences. However, this number can be trimmed to twelve basic sequences of signal processing. The basic rationale for choosing the sequences described below is to clearly illustrate the result of the acquisition logic changes instituted and tested in May, 1983. These twelve can be obtained by considering all permutations of the following three variables: (1) range interval, (2) scan status, and (3) AGC SET status. Range interval takes on the the three values: short, medium, and long. Scan status indicates whether a scan was initiated prior to an initial detection. AGC SET is a discrete internal to the EA-2 and is either high or low. During a given acquisition attempt, it is toggled high when the first "not-search" AGC is commanded into the control loop and is held high for the remainder of

Page intentionally left blank

Page intentionally left blank

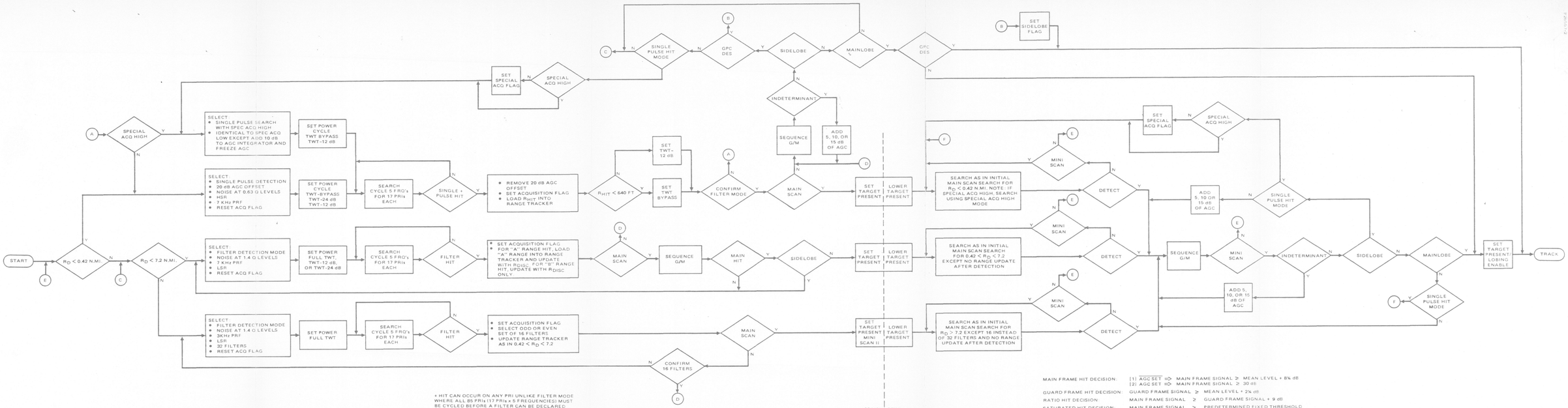

+ HIT CAN OCCUR ON ANY PRI UNLIKE FILTER MODE WHERE ALL 85 PRIs (17 PRIs x 5 FREQUENCIES) MUST BE CYCLED BEFORE A FILTER CAN BE DECLARED

TABLE 40-28A GPC ACQ AND DES* PASSIVE SEARCH AND ACQUISITION

*FOLLOW MAIN SCAN "N" PATH

MAIN FRAME HIT DECISION:	[1] $\overline{\text{AGC SET}}$ ⇒ MAIN FRAME SIGNAL ≥ MEAN LEVEL + 8% dB [2] AGC SET ⇒ MAIN FRAME SIGNAL ≥ 30 dB
GUARD FRAME HIT DECISION:	GUARD FRAME SIGNAL ≥ MEAN LEVEL + 2% dB
RATIO HIT DECISION:	MAIN FRAME SIGNAL ≥ GUARD FRAME SIGNAL + 9 dB
SATURATED HIT DECISION:	MAIN FRAME SIGNAL ≥ PREDETERMINED FIXED THRESHOLD (FUNCTION OF RANGE)
SIDELOBE DECISION:	GUARD HIT & $\overline{\text{RATIO HIT}}$ & $\overline{\text{SATURATED HIT}}$
MAINLOBE DECISION:	[1] MAIN HIT & $\overline{\text{GUARD HIT}}$ & $\overline{\text{AGC SET}}$ [2] MAIN HIT & RATIO HIT
INDETERMINANT DECISION:	$\overline{\text{SATURATED HIT}}$ & $\overline{\text{RATIO HIT}}$

Figure 3-1. GPC-ACQ and DES* Passive Search and Acquisition

Page intentionally left blank

Page intentionally left blank

the acquisition attempt. (Not-search AGC is defined as any AGC that is commanded as the result of guard frame processing. That is, the AGC can be increased by 0, +5, +10, or +15 dB as the result of guard processing, but it can never be decreased.)

Table 3-2 lists the twelve basic acquisition sequences and gives the table numbers providing the acquisition details for each case. Tables 3-3 through 3-14 give acquisition sequence details for all twelve cases. Note that the table is constructed so that the sequence of events progresses down the column of the table. For a given frame the following details are provided: the type of frame (main or guard), the scan process (main, mini, or neither), the AGC'd thermal noise level (if appropriate), the type of detector (fixed threshold or CFAR), the threshold level and its reference point, the number of range gates and their configuration, and the number of doppler filters per range gate (if applicable). The reader is cautioned that there are many variations of these twelve basic sequences, especially in the scanning cases. In these cases, the signal processing frames shown represent the last frames to occur in mainscan and miniscan. In reality, there can be hundreds of frames between the end of mainscan and the last three frames of miniscan, depending on the target size and range and target location relative to boresight at the time of mainscan termination.

TABLE 3-2. FUNDAMENTAL SIGNAL PROCESSING CONFIGURATIONS FOR GPC-ACQ, PASSIVE MODE

Range Interval	Scan Status	AGC Set Status	Table Number
Short	No	No	3-3
Short	Yes	No	3-4
Short	No	Yes	3-5
Short	Yes	Yes (mini only)	3-6
Medium	No	No	3-7
Medium	Yes	No	3-8
Medium	No	Yes	3-9
Medium	Yes	Yes	3-10
Long	No	No	3-11
Long	Yes	No	3-12
Long	No	Yes	3-13
Long	Yes	Yes (mini only)	3-14

TABLE 3-3. SIGNAL PROCESSING SEQUENCE FOR GPC-ACQ, PASSIVE, SHORT RANGE, NONSCANNING, NO AGC SET

Process	AGC'd Thermal Noise Level	Threshold	Range Gate Number	Range Gate Width	Doppler Filters per Range Gate
Signal Pulse	$(0.63q)^2$	4.5q Fixed	71	60 ft	--
Confirm (CFAR)	$(7q)^2$	8.25 dB (above M.L.)	2	3/2 T_p (overlap)	16
Guard (CFAR)	$(1.4q)^2$	2.25 dB (above M.L.)	2	3/2 T_p (overlap)	16
Main (CFAR)	$(1.4q)^2$	8.25 dB (above M.L.)	2	3/2 T_p (overlap)	16

TABLE 3-4. SIGNAL PROCESSING SEQUENCE FOR GPC-ACQ, PASSIVE, SHORT RANGE, SCANNING, NO AGC SET

Mainscan Process	Miniscan Process	AGC'd Thermal Noise Level	Threshold	Range Gate Number	Range Gate Width	Doppler Filters per Range Gate
Single Pulse		$(0.63q)^2$	4.5q Fixed	71	60 ft	--
Confirm (CFAR)		$(7q)^2$	8.25 dB (above M.L.)	2	3/2 T_p (overlap)	16
	Single Pulse	$(0.63q)^2$	4.5q Fixed	71	60 ft	--
	Confirm (CFAR)	$(7q)^2$	8.25 dB (above M.L.)	2	3/2 T_p (overlap)	16
	Guard (CFAR)	$(1.4q)^2$	2.25 dB (above M.L.)	2	3/2 T_p (overlap)	16
	Main (CFAR)	$(1.4q)^2$	8.25 dB (above M.L.)	2	3/2 T_p (overlap)	16

TABLE 3-5. SIGNAL PROCESSING SEQUENCE FOR GPC-ACQ, PASSIVE, SHORT RANGE, NONSCANNING, AGC SET

Process	AGC'd Thermal Noise Level	Threshold	Range Gate Number	Range Gate Width	Doppler Filters per Range Gate
Single Pulse	$(0.63q)^2$	4.5q Fixed	71	60 ft	--
Confirm (Fixed)	--	30 dB (l.c. output)	2	3/2 T_p (overlap)	16
Guard (CFAR)	--	2.25 dB (above M.L.)	2	3/2 T_p (overlap)	16
Main (Fixed)	--	30 dB (l.c. output)	2	3/2 T_p (overlap)	16

TABLE 3-6. SIGNAL PROCESSING SEQUENCE FOR GPC-ACQ, PASSIVE, SHORT RANGE, SCANNING, AGC SET

Mainscan Process	Miniscan Process	AGC'd Thermal Noise Level	Threshold	Range Gate Number	Range Gate Width	Doppler Filters per Range Gate
Single Pulse		$(0.63q)^2$	4.5q Fixed	71	60 ft	--
Confirm (CFAR)		$(7q)^2$	8.25 dB (above M.L.)	2	3/2 T_p (overlap)	16
	Single Pulse	$(0.63q)^2$	4.5q Fixed	71	60 ft	--
	Confirm (Fixed)	--	30 dB (l.c. output)	2	3/2 T_p (overlap)	16
	Guard (CFAR)	--	2.25 dB (above M.L.)	2	3/2 T_p (overlap)	16
	Main (Fixed)	--	30 dB (l.c. output)	2	3/2 T_p (overlap)	16

TABLE 3-7. SIGNAL PROCESSING SEQUENCE FOR GPC-ACQ, PASSIVE, MEDIUM RANGE, NONSCANNING, NO AGC SET

Process	AGC'd Thermal Noise Level	Threshold	Range Gate Number	Range Gate Width	Doppler Filters per Range Gate
Main (CFAR)	$(1.4q)^2$	8.25 dB (above M.L.)	2	3/2 T_p (overlap)	16
Guard (CFAR)	$(1.4q)^2$	2.25 dB (above M.L.)	2	3/2 T_p (overlap)	16
Main (CFAR)	$(1.4q)^2$	8.25 dB (above M.L.)	2	3/2 T_p (overlap)	16

TABLE 3-8. SIGNAL PROCESSING SEQUENCE FOR GPC-ACQ, PASSIVE, MEDIUM RANGE, SCANNING, NO AGC SET

Mainscan Process	Miniscan Process	AGC'd Thermal Noise Level	Threshold	Range Gate Number	Range Gate Width	Doppler Filters per Range Gate
Main (CFAR)		$(1.4q)^2$	8.25 dB (above M.L.)	2	3/2 T_p (overlap)	16
Guard (CFAR)		$(1.4q)^2$	2.25 dB (above M.L.)	2	3/2 T_p (overlap)	16
Main (CFAR)		$(1.4q)^2$	0 dB (above M.L.)	2	3/2 T_p (overlap)	16
	Main (CFAR)	$(1.4q)^2$	8.25 dB (above M.L.)	2	3/2 T_p (overlap)	16
	Guard (CFAR)	$(1.4q)^2$	2.25 dB (above M.L.)	2	3/2 T_p (overlap)	16
	Main (CFAR)	$(1.4q)^2$	8.25 dB (above M.L.)	2	3/2 T_p (overlap)	16

TABLE 3-9. SIGNAL PROCESSING SEQUENCE FOR GPC-ACQ, PASSIVE, MEDIUM RANGE, NONSCANNING, AGC SET

Process	AGC'd Thermal Noise Level	Threshold	Range Gate Number	Range Gate Width	Doppler Filters per Range Gate
Main (Fixed)	--	30 dB (l.c. output)	2	3/2 T_p (overlap)	16
Guard (CFAR)	--	2.25 dB (above M.L.)	2	3/2 T_p (overlap)	16
Main (Fixed)	--	30 dB (l.c. output)	2	3/2 T_p (overlap)	16

TABLE 3-10. SIGNAL PROCESSING SEQUENCE FOR GPC-ACQ, PASSIVE, MEDIUM RANGE, SCANNING, AGC SET

Mainscan Process	Miniscan Process	AGC'd Thermal Noise Level	Threshold	Range Gate Number	Range Gate Width	Doppler Filters per Range Gate
Main (Fixed)	--	--	30 dB (l.c. output)	2	3/2 T_p (overlap)	16
Guard (CFAR)	--	--	2.25 dB (above M.L.)	2	3/2 T_p (overlap)	16
Main (Fixed)	--	--	30 dB (l.c. output)	2	3/2 T_p (overlap)	16
	Main (Fixed)	--	30 dB (l.c. output)	2	3/2 T_p (overlap)	16
	Guard (CFAR)	--	2.25 dB (above M.L.)	2	3/2 T_p (overlap)	16
	Main (Fixed)	--	30 dB (l.c. output)	2	3/2 T_p (overlap)	16

TABLE 3-11. SIGNAL PROCESSING SEQUENCE FOR GPC-ACQ, PASSIVE, LONG RANGE, NONSCANNING, NO AGC SET

Process	AGC'd Thermal Noise Level	Threshold	Range Gate Number	Range Gate Width	Doppler Filters per Range Gate
Main (CFAR)	$(1.4q)^2$	8.25 dB (above M.L.)	2	3/2 T_p (overlap)	32
Guard (CFAR)	$(1.4q)^2$	2.25 dB (above M.L.)	2	3/2 T_p (overlap)	16
Main (CFAR)	$(1.4q)^2$	8.25 dB (above M.L.)	2	3/2 T_p (overlap)	16

TABLE 3-12. SIGNAL PROCESSING SEQUENCE FOR GPC-ACQ, PASSIVE, LONG RANGE, SCANNING, NO AGC SET

Mainscan Process	Miniscan Process	AGC'd Thermal Noise Level	Threshold	Range Gate Number	Range Gate Width	Doppler Filters per Range Gate
Main (CFAR)		$(1.4q)^2$	8.25 dB (above M.L.)	2	3/2 T_p (overlap)	32
	Main (CFAR)	$(1.4q)^2$	8.25 dB (above M.L.)	2	3/2 T_p (overlap)	16
	Guard (CFAR)	$(1.4q)^2$	2.25 dB (above M.L.)	2	3/2 T_p (overlap)	16
	Main (CFAR)	$(1.4q)^2$	8.25 dB (above M.L.)	2	3/2 T_p (overlap)	16

TABLE 3-13. SIGNAL PROCESSING SEQUENCE FOR GPC-ACQ, PASSIVE, LONG RANGE, NONSCANNING, AGC SET

Process	AGC'd Thermal Noise Level	Threshold	Range Gate Number	Range Gate Width	Doppler Filters per Range Gate
Main (CFAR)	$(1.4q)^2$	8.25 dB (above M.L.)	2	3/2 T_p (overlap)	32
.		.			.
.		.			.
.		.			.
Guard (CFAR)	--	2.25 dB (above M.L.)	2	3/2 T_p (overlap)	16
Main (Fixed)	--	30 dB (l.c. output)	2	3/2 T_p (overlap)	16

TABLE 3-14. SIGNAL PROCESSING SEQUENCE FOR GPC-ACQ, PASSIVE, LONG RANGE, SCANNING, AGC SET

Mainscan Process	Miniscan Process	AGC'd Thermal Noise Level	Threshold	Range Gate Number	Range Gate Width	Doppler Filters per Range Gate
Main (CFAR)		$(1.4q)^2$	8.25 dB (above M.L.)	2	3/2 T_p (overlap)	32
	.		.			.
	.		.			.
	.		.			.
	Main (Fixed)	—	30 dB (l.c. output)	2	3/2 T_p (overlap)	16
	Guard (CFAR)	--	2.25 dB (l.c. output)	2	3/2 T_p (overlap)	16
	Main (Fixed)	--	30 dB (l.c. output)	2	3/2 T_p (overlap)	16

3.4 AUTO, PASSIVE MODE

Only one computer model is used for the auto, passive mode. Figure 3-2, taken from Reference [7], summarizes the search and acquisition logic for this mode. As in the GPC-ACQ passive case, it is useful to provide the signal processing details for a fundamental set of sequences. Definition of this fundamental set is somewhat arbitrary and we proposed it take the following form. The set will consist of all permutations of the range interval, scan status, and AGC SET status. Scan status and AGC SET status are both two state discretes and take on the same meaning as in the GPC-ACQ, passive mode discussion. The range interval takes on two states: short or determinant. Short range implies that the initial detection (or alert) was determined to be at short range, i.e., less than 2560 feet. Determinant range implies that the initial detection was greater than approximately 35000 feet. These two states do not cover a third range interval from 2560 feet to approximately 35000 feet. This interval is known internally to the EA-2 as the indeterminant range interval. We will ignore this interval in our summary because the processing sequence for this interval is too complicated to summarize in a single table.

Table 3-15 summarizes the eight possible permutations of these three discrete variables and provides the table number for each case. Tables 3-16 through 3-23 give the signal processing sequence details for each case.

3.5 ACTIVE MODE

Only one computer model is used for the active mode. The search and acquisition logic for this mode is summarized in Figure 3-3 and was copied from Reference [7]. As in the previous two cases, we have identified a fundamental set of signal processing sequences that covers most active mode situations of interest. Again this set consists of all permutations of the parameters: range interval, scan status, and AGC SET status. In the active case, range interval takes on two states: range >49920 feet and range <49920 feet, and scan status and AGC SET status have the same meaning as before. This gives a total of eight possible permutations.

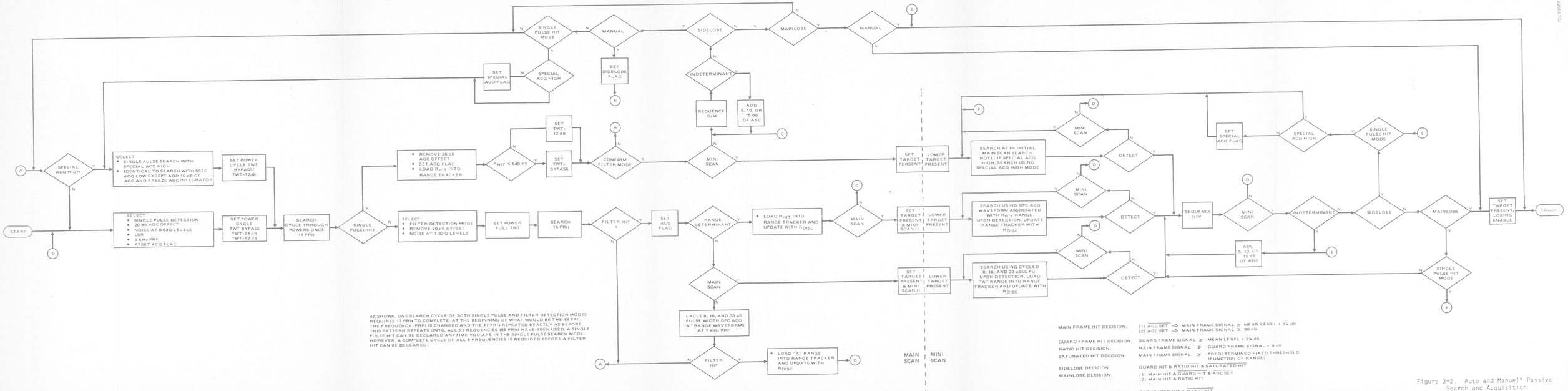

AS SHOWN, ONE SEARCH CYCLE OF BOTH SINGLE PULSE AND FILTER DETECTION MODES REQUIRES 17 PRIs TO COMPLETE. AT THE BEGINNING OF WHAT WOULD BE THE 18 PRI, THE FREQUENCY (PRF) IS CHANGED AND THE 17 PRIs REPEATED EXACTLY AS BEFORE. THIS PATTERN REPEATS UNTIL ALL 5 FREQUENCIES (85 PRIs) HAVE BEEN USED. A SINGLE PULSE HIT CAN BE DECLARED ANYTIME YOU ARE IN THE SINGLE PULSE SEARCH MODE. HOWEVER, A COMPLETE CYCLE OF ALL 5 FREQUENCIES IS REQUIRED BEFORE A FILTER HIT CAN BE DECLARED.

MAIN FRAME HIT DECISION:	(1) $\overline{\text{AGC SET}}$ ⇒ MAIN FRAME SIGNAL ≥ MEAN LEVEL + 8¼ dB (2) AGC SET ⇒ MAIN FRAME SIGNAL ≥ 30 dB
GUARD FRAME HIT DECISION:	GUARD FRAME SIGNAL ≥ MEAN LEVEL + 2¼ dB
RATIO HIT DECISION:	MAIN FRAME SIGNAL ≥ GUARD FRAME SIGNAL + 9 dB
SATURATED HIT DECISION:	MAIN FRAME SIGNAL ≥ PREDETERMINED FIXED THRESHOLD (FUNCTION OF RANGE)
SIDELOBE DECISION:	GUARD HIT & $\overline{\text{RATIO HIT}}$ & $\overline{\text{SATURATED HIT}}$
MAINLOBE DECISION:	(1) MAIN HIT & $\overline{\text{GUARD HIT}}$ & AGC SET (2) MAIN HIT & $\overline{\text{RATIO HIT}}$
INDETERMINANT DECISION:	$\overline{\text{SATURATED HIT}}$ & $\overline{\text{RATIO HIT}}$

Figure 3-2. Auto and Manual* Passive Search and Acquisition

Page intentionally left blank

Page intentionally left blank

TABLE 3-15. FUNDAMENTAL SIGNAL PROCESSING CONFIGURATIONS FOR THE AUTO, PASSIVE MODE

Range Interval	Scan Status	AGC SET Status	Table Number
Short	No	No	3-16
Short	Yes	No	3-17
Short	No	Yes	3-18
Short	Yes	Yes	3-19
Determinant	No	No	3-20
Determinant	Yes	No	3-21
Determinant	No	Yes	3-22
Determinant	Yes	Yes	3-23

TABLE 3-16. SIGNAL PROCESSING SEQUENCE FOR AUTO, PASSIVE, SHORT RANGE, NONSCANNING, NO AGC SET

Process	AGC'd Thermal Noise Level	Threshold	Range Gate Number	Range Gate Width	Doppler Filters per Range Gate
Single Pulse/CFAR	$(0.63q)^2$/ $(1.4q)^2$	4.5q Fixed/ 8.25 dB (above M.L.)	71/ 4	60 ft/T_p	--/ 16
(Single Pulse Hi					
Confirm (CFAR)	$(7q)^2$	8.25 dB (above M.L.)	2	3/2 T_p (overlap)	16
Guard (CFAR)	$(1.4q)^2$	2.25 dB (above M.L.)	2	3/2 T_p (overlap)	16
Main (CFAR)	$(1.4q)^2$	8.25 dB (above M.L.)	2	3/2 T_p (overlap)	16

TABLE 3-17. SIGNAL PROCESSING SEQUENCE FOR AUTO, PASSIVE, SHORT RANGE, SCANNING, NO AGC SET

Mainscan Process	Miniscan Process	AGC'd Thermal Noise Level	Threshold	Range Gate Number	Range Gate Width	Doppler Filters per Range Gate
Single Pulse/ CFAR		$(0.63q)^2$/ $(1.4q)^2$	4.5q Fixed/ 8.25 dB (above M.L.)	71/ 4	60 ft/T_p	--/ 16
(Single Pulse Hit)						
Confirm (CFAR)		$(7q)^2$	8.25 dB (above M.L.)	2	3/2 T_p (overlap)	16
	Single Pulse/ CFAR	$(0.63q)^2$ $(1.4q)^2$	4.5q Fixed/ 8.25 dB (above M.L.)	71/ 4	60 ft/T_p	--/ 16
	Confirm (CFAR)	$(7q)^2$	8.25 dB (above M.L.)	2	3/2 T_p (overlap)	16
	Guard (CFAR)	$(1.4q)^2$	2.25 dB (above M.L.)	2	3/2 T_p (overlap)	16
	Main (CFAR)	$(1.4q)^2$	8.25 dB (above M.L.)	2	3/2 T_p (overlap)	16

TABLE 3-18. SIGNAL PROCESSING SEQUENCE FOR AUTO, PASSIVE, SHORT RANGE, NONSCANNING, AGC SET

Process	AGC'd Thermal Noise Level	Threshold	Range Gate Number	Range Gate Width	Doppler Filters per Range Gate
Single Pulse/ Fixed	—	4.5q (Fixed)/ 30 dB (l.c. output)	71/ 4	60 ft/T_p	--/ 16
(Single Pulse Hit)					
Confirm (Fixed)	--	30 dB (l.c. output)	2	3/2 T_p (overlap)	16
Guard (CFAR)	--	2.25 dB (above M.L.)	2	3/2 T_p (overlap)	16
Main (Fixed)	--	30 dB (l.c. output)	2	3/2 T_p (overlap)	16

TABLE 3-19. SIGNAL PROCESSING SEQUENCE FOR AUTO, PASSIVE, SHORT RANGE, SCANNING, AGC SET

Mainscan Process	Miniscan Process	AGC'd Thermal Noise Level	Threshold	Range Gate Number	Range Gate Width	Doppler Filters per Range Gate
Single Pulse/ (CFAR)		--	4.5q Fixed/ 8.25 dB (above M.L.)	71/ 4	60 ft/T_p	--/ 16
(Single Pulse Hit)						
Confirm (CFAR)		--	8.25 dB (above M.L.)	2	3/2 T_p (overlap)	16
	Single Pulse/ (Fixed)	--	4.5q Fixed/ 30 dB (l.c. output)	71/ 4	3/2 T_p (overlap)	16
	Confirm (Fixed)	--	30 dB (l.c. output)	2	3/2 T_p (overlap)	16
	Guard (CFAR)	--	2.25 dB (above M.L.)	2	3/2 T_p (overlap)	16
	Main (CFAR)	--	30 dB (l.c. output)	2	3/2 T_p (overlap)	16

TABLE 3-20. SIGNAL PROCESSING SEQUENCE FOR AUTO, PASSIVE, DETERMINANT RANGE, NONSCANNING, NO AGC SET

Process	AGC'd Thermal Noise Level	Threshold	Range Gate Number	Range Gate Width	Doppler Filters per Range Gate
Single Pulse/ CFAR	$(0.63q)^2$ $(1.4q)^2$	4.5q Fixed/ 8.25 dB (above M.L.)	71/ 4	60 ft/T_p	--/ 16
(Determinant Hit)					
Guard (CFAR)	$(1.4q)^2$	2.25 dB (above M.L.)	2	3/2 T_p (overlap)	16
Main (CFAR)	$(1.4q)^2$	8.25 dB (above M.L.)	2	3/2 T_p (overlap)	16

TABLE 3-21. SIGNAL PROCESSING SEQUENCE FOR AUTO, PASSIVE, DETERMINANT RANGE, NONSCANNING, NO AGC SET

Mainscan Process	Miniscan Process	AGC'd Thermal Noise Level	Threshold	Range Gate Number	Range Gate Width	Doppler Filters per Range Gate
Single Pulse/ CFAR		$(0.63q)^2$ $(1.4q)^2$	4.5q Fixed/ 8.25 dB (above M.L.)	71/ 4	60 ft/T_p	--/ 16
(Determinant Hit)						
	. . .		. . .			. . .
	Main (CFAR)	$(1.4q)^2$	8.25 dB (above M.L.)	2	3/2 T_p (overlap)	16
	Guard (CFAR)	$(1.4q)^2$	2.25 dB (above M.L.)	2	3/2 T_p (overlap)	16
	Main (CFAR)	$(1.4q)^2$	8.25 dB (above M.L.)	2	3/2 T_p (overlap)	16

TABLE 3-22. SIGNAL PROCESSING SEQUENCE FOR AUTO, PASSIVE, DETERMINANT RANGE, NONSCANNING, AGC SET

Process	AGC'd Thermal Noise Level	Threshold	Range Gate Number	Range Gate Width	Doppler Filters per Range Gate
Single Pulse/ Fixed	--	4.5q Fixed/ 30 dB (l.c. output)	71/ 4	60 ft/T_p	--/ 16
(Determinant Hit)					
Guard (CFAR)	--	2.25 dB (above M.L.)	2	3/2 T_p (overlap)	16
Main (Fixed)	--	30 dB (l.c. output)	2	3/2 T_p (overlap)	16

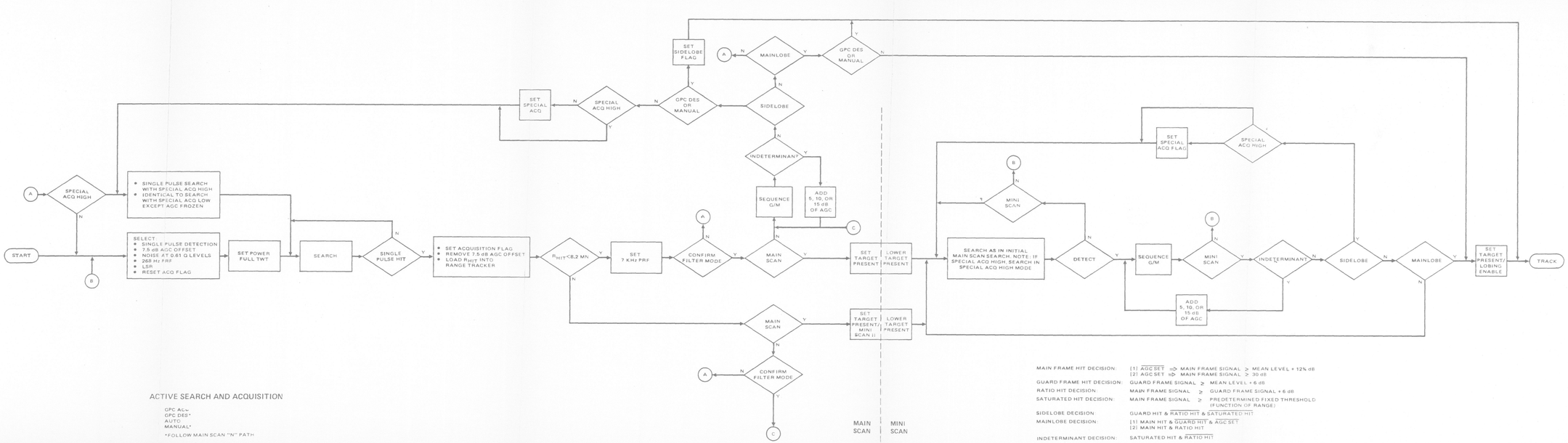

ACTIVE SEARCH AND ACQUISITION

GPC ACQ*
GPC DES*
AUTO
MANUAL*

*FOLLOW MAIN SCAN "N" PATH

MAIN FRAME HIT DECISION:	(1) $\overline{\text{AGC SET}}$ ⇒ MAIN FRAME SIGNAL ≥ MEAN LEVEL + 12% dB (2) AGC SET ⇒ MAIN FRAME SIGNAL ≥ 30 dB
GUARD FRAME HIT DECISION:	GUARD FRAME SIGNAL ≥ MEAN LEVEL + 6 dB
RATIO HIT DECISION:	MAIN FRAME SIGNAL ≥ GUARD FRAME SIGNAL + 6 dB
SATURATED HIT DECISION:	MAIN FRAME SIGNAL ≥ PREDETERMINED FIXED THRESHOLD (FUNCTION OF RANGE)
SIDELOBE DECISION:	GUARD HIT & $\overline{\text{RATIO HIT}}$ & $\overline{\text{SATURATED HIT}}$
MAINLOBE DECISION:	(1) MAIN HIT & $\overline{\text{GUARD HIT}}$ & $\overline{\text{AGC SET}}$ (2) MAIN HIT & $\overline{\text{RATIO HIT}}$
INDETERMINANT DECISION:	SATURATED HIT & $\overline{\text{RATIO HIT}}$

Figure 3-3. Active Search and Acquisition

Page intentionally left blank

Page intentionally left blank

TABLE 3-23. SIGNAL PROCESSING SEQUENCE FOR AUTO, PASSIVE, DETERMINANT RANGE, SCANNING, AGC SET

Mainscan Process	Miniscan Process	AGC'd Thermal Noise Level	Threshold	Range Gate Number	Range Gate Width	Doppler Filters per Range Gate
Single Pulse/ CFAR		--	4.5q Fixed 8.25 dB (above M.L.)	71/ 4	60 ft/T_p	--/ 16
(Determinant Hit)						
	. . .		. . .			. . .
	Main (Fixed)	--	30 dB (l.c. output)	2	3/2 T_p (overlap)	16
	Guard (CFAR)	--	2.25 dB (above M.L.)	2	3/2 T_p (overlap)	16
	Main (Fixed)	--	30 dB (l.c. output)	2	3/2 T_p (overlap)	16

Table 3-24 summarizes the eight permutations and provides table numbers for each case. Tables 3-25 through 3-32 give the details of the signal processing sequence for each of the eight fundamental cases.

TABLE 3-24. FUNDAMENTAL SIGNAL PROCESSING CONFIGURATIONS FOR THE ACTIVE MODE

Range Interval, feet	Scan Status	AGC Set Status	Table Number
R < 49920	No	No	3-25
R < 49920	Yes	No	3-26
R < 49920	No	Yes	3-27
R < 49920	Yes	Yes	3-28
R > 49920	No	No	3-29
R > 49920	Yes	No	3-30
R > 49920	No	Yes	3-31
R > 49920	Yes	Yes (mini only)	3-32

TABLE 3-25. SIGNAL PROCESSING SEQUENCE FOR ACTIVE, R < 49920 FEET, NONSCANNING, NO AGC SET

Process	AGC'd Thermal Noise Level	Threshold	Range Gate Number	Range Gate Width	Doppler Filters per Range Gate
Single Pulse (Hit < 49920')	$(0.61q)^2$	4.5q Fixed	1787	1020 ft	--
Confirm (CFAR-7 kHz)	$(1.4q)^2$	12 dB (above M.L.)	2	3/2 T_p (overlap)	16
Guard (CFAR-7 kHz)	$(1.4q)^2$	6 dB (above M.L.)	2	3/2 T_p (overlap)	16
Main (CFAR-7 kHz)	$(1.4q)^2$	12 dB (above M.L.)	2	3/2 T_p (overlap)	16

TABLE 3-26. SIGNAL PROCESSING SEQUENCE FOR ACTIVE, R < 49920 FEET, SCANNING, NO AGC SET

Mainscan Process	Miniscan Process	AGC'd Thermal Noise Level	Threshold	Range Gate Number	Range Gate Width	Doppler Filters per Range Gate
Single Pulse (Hit < 49920')		$(0.61q)^2$	4.5q Fixed	1787	1020 ft	--
Confirm (CFAR-7 kHz)		$(1.4q)^2$ (above M.L.)	12 dB	2	3/2 T_p (overlap)	16
	Single Pulse	$(0.61q)^2$	4.5q Fixed	1787	3/2 T_p (overlap)	16
	Confirm (CFAR-7 khz)	$(1.4q)^2$	12 dB (above M.L.)	2	3/2 T_p (overlap)	16
	Guard (CFAR-7 khz)	$(1.4q)^2$	6 dB (above M.L.)	2	3/2 T_p (overlap)	16
	Main (CFAR-7 khz)	$(1.4q)^2$	12 dB (above M.L.)	2	3/2 T_p (overlap)	16

TABLE 3-27. SIGNAL PROCESSING SEQUENCE FOR ACTIVE, R < 49920 FEET, NONSCANNING, AGC SET

Process	AGC'D Thermal Noise Level	Threshold	Range Gate Number	Range Gate Width	Doppler Filters per Range Gate
Single Pulse (Hit < 49920')	--	4.5q Fixed	1787	1020 ft	--
Confirm (Fixed-7 kHz)	--	30 dB (l.c. output)	2	3/2 T_p (overlap)	16
Guard (CFAR-7 kHz)	--	6 dB (above M.L.)	2	3/2 T_p (overlap)	16
Main (Fixed-7 kHz)	--	30 dB (l.c. output)	2	3/2 T_p (overlap)	16

TABLE 3-28. SIGNAL PROCESSING SEQUENCE FOR ACTIVE, R < 49920 FEET, SCANNING, AGC SET

Mainscan Process	Miniscan Process	AGC'D Thermal Noise Level	Threshold	Range Gate Number	Range Gate Width	Doppler Filters per Range Gate
Single Pulse (Hit < 49920')		$(0.61q)^2$	4.5q Fixed	1787	1020 ft	--
Confirm (CFAR-7 kHz)		$(1.4q)^2$	12 dB (above M.L.)	2	3/2 T_p (overlap)	16
	Single Pulse	—	4.5q Fixed	1787	1020 ft	--
	Confirm (Fixed-7 kHz)	--	30 dB (l.c. output)	2	3/2 T_p (overlap)	16
	Guard (CFAR-7 kHz)	--	6 dB (above M.L.)	2	3/2 T_p (overlap)	16
	Main (Fixed-7 kHz)	--	30 dB (l.c. output)	2	3/2 T_p (overlap)	16

TABLE 3-29. SIGNAL PROCESSING SEQUENCE FOR ACTIVE, R > 49920 FEET, NONSCANNING, NO AGC SET

Process	AGC'd Thermal Noise Level	Threshold	Range Gate Number	Range Gate Width	Doppler Filters per Range Gate
Single Pulse (Hit > 49920')	$(0.61q)^2$	4.5q Fixed	1787	1020 ft	--
Confirm (CFAR-268 Hz)	$(1.4q)^2$	12 dB (above M.L.)	2	3/2 T_p (overlap)	16
Guard (CFAR-268 Hz)	$(1.4q)^2$	6 dB (above M.L.)	2	3/2 T_p (overlap)	16
Main (CFAR-268 Hz)	$(1.4q)^2$	12 dB (above M.L.)	2	3/2 T_p (overlap)	16

TABLE 3-30. SIGNAL PROCESSING SEQUENCE FOR ACTIVE, R > 49920 FEET, SCANNING, NO AGC SET

Mainscan Process	Miniscan Process	AGC'd Thermal Noise Level	Threshold	Range Gate Number	Range Gate Width	Doppler Filters per Range Gate
Single Pulse (Hit > 49920')		$(0.61q)^2$	4.5q Fixed	1787	1020 ft	--
	. . .		. . .		. . .	
	Single Pulse	$(0.61q)^2$	4.5q Fixed	1787	1020 ft	--
	Confirm (CFAR-268 Hz)	$(1.4q)^2$	12 dB (above M.L.)	2	3/2 T_p (overlap)	16
	Guard (CFAR-268 Hz)	$(1.4q)^2$	6 dB (above M.L.)	2	3/2 T_p (overlap)	16
	Main (CFAR-268 Hz)	$(1.4q)^2$	12 dB (above M.L.)	2	3/2 T_p (overlap)	16

TABLE 3-31. SIGNAL PROCESSING SEQUENCE FOR ACTIVE, R > 49920 FEET, NONSCANNING, AGC SET

Process	AGC'D Thermal Noise Level	Threshold	Range Gate Number	Range Gate Width	Doppler Filters per Range Gate
Single Pulse (Hit > 49920')	--	4.5q Fixed	1787	1020 ft	--
Confirm (Fixed-268 Hz)	--	30 dB (l.c. output)	2	3/2 T_p (overlap)	16
Guard (CFAR-268 Hz)	--	6 dB (above M.L.)	2	3/2 T_p (overlap)	16
Main (Fixed-268 Hz)	--	30 dB (l.c. output)	2	3/2 T_p (overlap)	16

TABLE 3-32. SIGNAL PROCESSING SEQUENCE FOR ACTIVE, R > 49920 FEET, SCANNING, AGC SET

Mainscan Process	Miniscan Process	AGC'd Thermal Noise Level	Threshold	Range Gate Number	Range Gate Width	Doppler Filters per Range Gate
Single Pulse (Hit > 49920')		$(0.61q)^2$	4.5q Fixed	1787	1020 ft	--
	. . .		. . .		. . .	. . .
	Single Pulse	--	4.5q Fixed	1787	1020 ft	--
	Confirm (Fixed-268 Hz)	--	30 dB (l.c. output)	2	3/2 T_p	16
	Guard (CFAR-268 Hz)	--	6 dB (above M.L.)	2	3/2 T_p	16
	Main (Fixed-268 Hz)	--	30 dB (l.c. output)	2	3/2 T_p	16

4. SPACECRAFT RCS MODEL DETAILS

This section provides detailed descriptions of the three new spacecraft RCS models developed since July 1980. In form, the models basically parallel the form of the SPAS RCS computer model described in detail in Reference [1]. However, some modifications had to be made to the original form. These modifications stem from the fact that the structure of SPAS was such that normals to all flat surfaces lie along the spacecraft coordinate axes. In the three spacecraft models described herein, we did not have that luxury. The implication of this is that the method of determining the illumination of a point target, representing a flat surface, had to be generalized. Additionally, the method for computing the wander vectors associated with the diffuse scatterers had to be generalized.

This section is structured in the following way. First, a review of the general RCS modeling method is presented. Next, a step-by-step description of the construction of the individual point scatterer parameters for a given spacecraft is presented. Then, the results of these constructions are provided for the three new spacecraft models: LDEF, SMMS, and Space Telescope.

4.1 REVIEW OF GENERAL RCS MODELING METHOD

The general RCS modeling method represents the spacecraft as a collection of point scatterers whose cross-section amplitude functions are assigned by rules described below and whose phases are determined by the spatial separation of the various point target locations. The collection of points are divided into two groups: those representing simple geometrical shapes, (e.g., plates, spheres, and cylinders) and those that do not. Those points that do not represent simple geometrical shapes are designed to represent a rectangular, rough-surfaced area with the appropriate cross-section functions and scattering center motion.

4.1.1 Description of Scatterers Representing Simple Geometrical Shapes

Both the location of the scattering point and the cross section functional form are highly dependent upon the shape being represented. Consider the choice of the location for the scattering point. For all flat, conducting plates the point scatterer location is chosen to be the center of the plate. For parabolic dish antennas, the point is placed at the phase center of the antenna. Finally, consider a conducting sphere for which geometric optics applies, the scattering center requires three pieces of information in order to compute the location of the scattering center: (1) the location of the sphere center, (2) the radius of the sphere, and (3) the line-of-sight (LOS) vector from the sphere center toward the radar. Items (1) and (2) can be computed a priori, but (3) must be computed during a simulation run. While there are many more simple geometric shapes, the three examples given above represented the majority of the scatterers on the four satellite models developed.

Next, consider the assignment of the cross-section amplitude function for each geometric scatterer. In general, this function varies with aspect angle. However, for all geometric scatterer types, the following rule was used in order to maintain computation simplicity. The scatterer was assumed to provide a constant cross section over those aspect angles for which theory gives a significant value and zero outside this region. For example, consider flat plates and parabolic dish antennas; the region of nonzero cross-section is taken to be the 3 dB-to-3 dB width of the mainlobe. One final note on assigning cross section values, depending on the material covering the surface, one might use the maximum cross section value obtained from theory if the surface is smooth or the value might be adjusted downward by as much as 20 dB if the surface is rough or "crinkled." There is still significant guesswork in the assignment of these values.

4.1.2 Description of Scatterers Representing Rough Surfaces

All areas of a given spacecraft represented by rough-surface models are broken into convenient subareas which are rectangular in shape. Each of these rectangular subareas is replaced by a point scatterer and a cross-section amplitude function as in the simple-geometric scatterer case. At long ranges,

where the antenna 3 dB-to-3 dB beam width is much larger than the target extent, the point location for a given subarea is taken as fixed at the center of the rectangle. However, at close range, the point is moved randomly from data cycle to data cycle in order to avoid the possibility of no beam wander when only one point target is within the beam. Rules for updating the random motion of the point location are described in Appendix F of Reference [1].

Assignment of a cross-section function was discussed in Section 4 of Reference [1] and is reiterated here. The cross section amplitude function assigned to the rough-surface area is identical to that used for ground scattering. That is, the maximum return is assumed to occur at normal incidence and falls off as the cosine of the angle off the normal. The backscatter coefficient, or the cross section at normal incidence was somewhat arbitrarily assigned a value of -10 dB and this value was then randomized among the rectangular, rough-surface scatterers as follows:

$$RCS(i) = -10 \text{ dB} + 0.1\,(u(0,1) - 0.5) \qquad (4\text{-}1)$$

where

RCS(i) = backscatter coefficient for ith rough-surface scatterers,
u(0,1) = uniform random number generation on (0,1).

The choice of -10 dB, while arbitrary, appears to be a very reasonable number upon comparing computer RCS predictions and flight data from STS-7, -11, and -13.

4.2 CONSTRUCTION OF A POINT SCATTERER MODEL FOR A GENERAL SPACECRAFT

This section provides a description of the general procedure for constructing the point scatterer parameters for a given spacecraft. The basic steps of the procedure are summarized below.

1. Choose a convenient coordinate system.
2. Assign each scattering surface of the spacecraft to the simple geometric category or the rough-surface category.

3. Determine point locations using the rules outlined in Sections 4.1.1 and 4.1.2.

4. Assign a maximum cross section value to each point scatterer, using the rules outlined in Sections 4.1.1 and 4.1.2.

5. Determine a normal vector for all point scatterers representing flat or rectangular rough surfaces.

6. Compute shadow region parameters for targets affected by the phenomenon. (This will usually only include targets with a significant RCS over a large aspect angle.)

7. Compute Euler angles required to transform the spacecraft coordinates to a coordinate system fixed on the individual scatterer with z-axis along the normal. (This computation only applies to flat surfaces and rough-surface scatterers.)

Steps 1 through 4 of the procedure are fairly straight forward. Steps 5 through 7 represent a generalization of the procedure used when modeling the Shuttle Pallet Satellite (SPAS). The generalization arises because many of the flat plate and rough-surface models for the three new spacecrafts no longer have normals parallel to the principle axes of the spacecraft coordinate system.

4.2.1 Construction Procedure

The first step is to choose a convenient coordinate systems. Its origin should be placed so that as many of the coordinate axes can be aligned with symmetry axes of the spacecraft.

Next, from a detailed description of the spacecraft, determine which objects should be represented as simple geometric shapes and which objects should be represented as rough-surface scatterers. Note that the rough-surface area should be divided into convenient rectangular areas and that the resulting rectangles do not need to be the same size.

Once all of the scatterers have been identified, the location of the scattering centers are determined for each target using the rules outlined in Sections 4.1.1 and 4.1.2 and a detailed blueprint of the spacecraft. Notice that for truncated cylinders and spheres, the geometric center and radius is used to determine the point scatterer location, so both quantities must be measured for these two shapes.

Each scatterer is now assigned a maximum cross-section value using the rules of Section 4.1. This step requires a lot of experience and guesswork. For example, if a flat rectangular plate is covered with slightly crinkled foil, it is not clear just how much one should degrade the peak of the mainlobe from that of a smooth conductor. Nor is it clear just exactly how much the mainlobe should be broadened when degrading its peak.

The next three steps (Steps 5 through 7) determine parameters used to decide when a given scatterer has a nonzero RCS in the direction of the radar. This deviates from the original procedure used for SPAS. We will first describe the original procedure and then we will give the new more generalized procedure.

The original procedure took advantage of the fact that all rough-surfaced scatterers had normals aligned with principal axes of the coordinate system and that all simple geometric-shaped scatterers had symmetry axes aligned with the principle axes of the coordinate system. One can then easily define a region of nonzero RCS for a given point scatterer, which accounts (fairly accurately) for the effects of shadowing as well, by defining a minimum and maximum value for each component of the unit vector in the direction of the radar. (The RCS will be nonzero if all components of the unit vector are simultaneously within the interval defined by their respective minimum-maximum pair.) Hence, each point target required a measurement of six angles to determine a nonzero RCS region that includes shadowing from neighboring surfaces.

In order to model the remaining spacecrafts, the above procedure was generalized as follows. First, the unit vector in the direction of the radar was transformed to a coordinate system whose x-y axes are aligned with the symmetry axes of the given object (and whose z-axis is normal to the surface if the object is a flat plate or a rough-surface scatterer). Then, an identical procedure to that described in the previous paragraph was applied to determine the region of nonzero RCS values in point scatterer coordinates. This new procedure requires three pairs of minimum and maximum angles in the convenient new coordinate system and it requires a determination of the three Euler angles to transform to the convenient coordinate system. Thus, the generalization has required the determination of an additional three numbers per target.

The Euler transformation is utilized in another part of the model as well. The equations used to update the random motion of the point scatterer representing a rough, rectangular surface were also generalized to include surfaces whose normals are not aligned with the spacecraft coordinates. The generalization was to update the random motion in the convenient target coordinate system (with z-normal to the surface) and then apply the inverse Euler transformation matrix to obtain the scatterer location in spacecraft coordinates.

4.2.2 Long Duration Exposure Facility (LDEF) Model

LDEF is a long, 12-sided cylinder shaped spacecraft. As shown in Figure 4-1, it is approximately 30 feet long and 14 feet in diameter. Its frame provides a matrix of identically shaped slots in which trays of individual experiments are placed. Figure 4-2 depicts the "unfolded" matrix of slots along the length of the cylinder, while Figure 4-3 gives the slot arrangements for the ends of the cylinder. Notice the slots in these figures are labeled for convenience in describing the computer model. Also, notice that the slots have various cross-hatch codings on them. There are three types of slot utilization indicated by different coding: (1) a tray covered with a flat plate is fit in the slot with the plate cover flush with the outer surface of the LDEF structure, (2) a tray with a recessed (6 inches) cover is

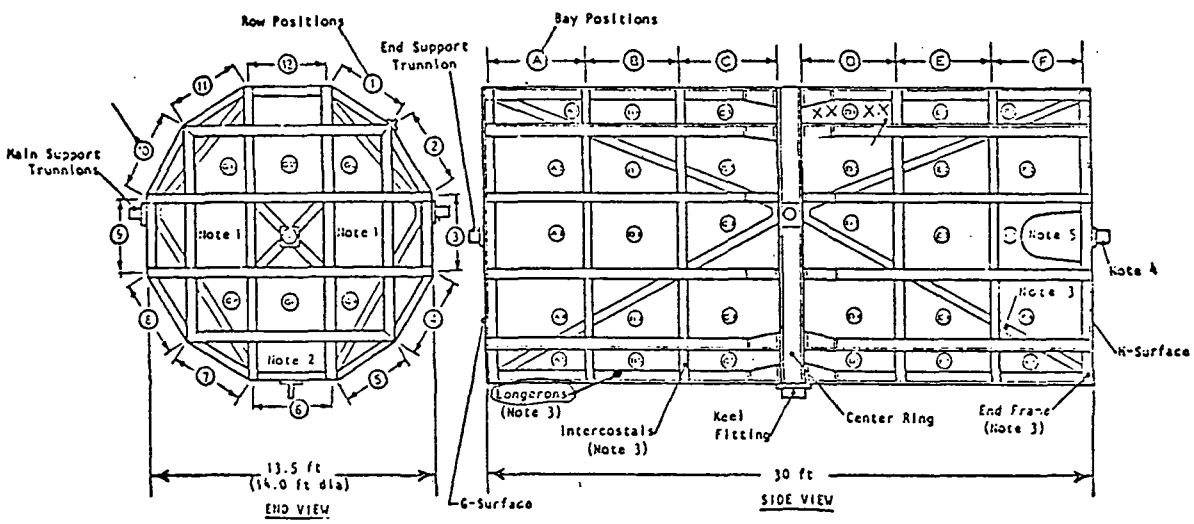

Figure 4-1. The LDEF Structure

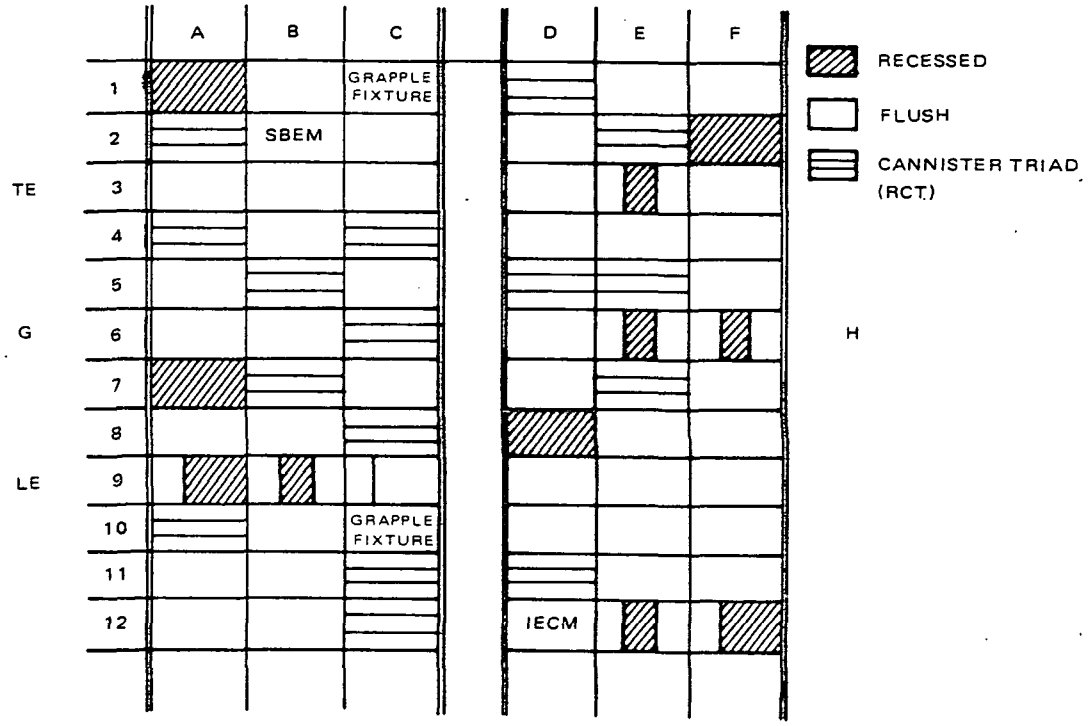

Figure 4-2. Typical Arrangement of Experiment Trays on LDEF

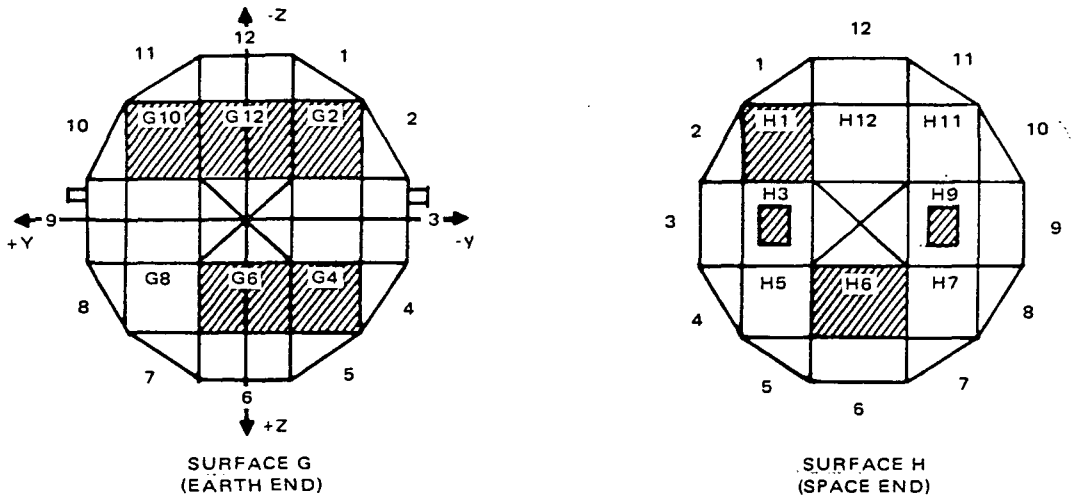

Figure 4-3. Typical Arrangement of Experiment Trays on LDEF End Panels

fit in the slot with the lip of the tray flush with the outer surface of LDEF, and (3) three parallel cannisters are placed in the tray with no cover and placed in the slot so that the lip of the tray is flush with the outer structure of LDEF. These three tray types are illustrated in detail in Figure 4-4. The distribution of tray types shown in Figures 4-2 and 4-3 was used in the development of the LDEF RCS computer model. However, the reader should note that this distribution represented the LDEF manufacturer's best estimate of the slot utilization at the time of RCS model development.

The first step in modeling the LDEF is the identification of an appropriate coordinate system as shown in Figure 4-5. X-axis of the coordinate system is coincident with the cylinder axis. The origin is chosen to lie at the midpoint of the cylinder with minus-x protruding from the G-surface and the positive x-axis protruding from the H-surface. The y and z axes are defined as follows. Plus-y emerges from the center of the surface defining row 9, while minus-y emerges from the center of the surface defining row 3. Plus-z emerges from the center of the surface defining row 6 and minus-z emerges from the center of the surface defining row 12. Next, the rough-surface scatterers and the simple geometric scatterers are identified. For the rough-surface scatterers, each of the 12 rows of slots was divided into two rectangular scattering areas butted end-to-end and the ends of the cylinder were each treated as a single rectangular scattering area. This arrangement is illustrated in Figure 4-6.

Simple geometric scatterers were identified using the following modeling rules for the three tray types. The flush planar surface tray is treated as a flat, rectangular conducting plate. The recessed planar surface tray is modeled as a flat, rectangular conducting plate. We note that the angle on the exposed lip of the tray precludes the need for including a corner reflector in this model. Finally, the tray configuration known as the recessed cannister triad is modeled as three parallel truncated cylinders with appropriate shadowing included. Figures 4-7 through 4-9 identify by number the individual point scatterers. Table 4-1 summarizes the geometric shape assumed for each of these scatterers. Notice that the LDEF spacecraft is represented by a total of 189 point scatterers.

8A. RECESSED PLANAR SURFACE

(CROSS-HATCHED MARKING DENOTES EXTENT OF EXPERIMENT VOLUME)

VISIBLE:
33" X 48.75" PLATE RECESSED 6"

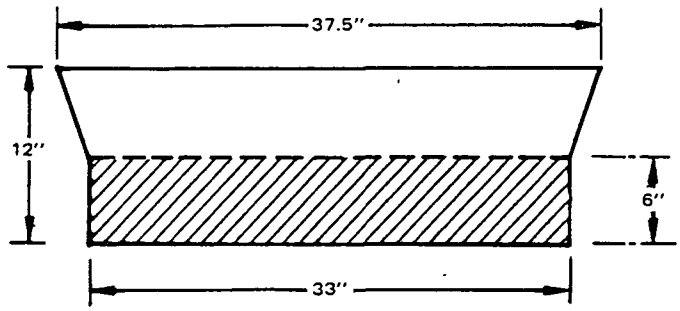

8B. FLUSH PLANAR SURFACE

VISABLE
37.5" X 48.75" PLATE FLUSH WITH LDEF STRUCTURAL PERIPHERY

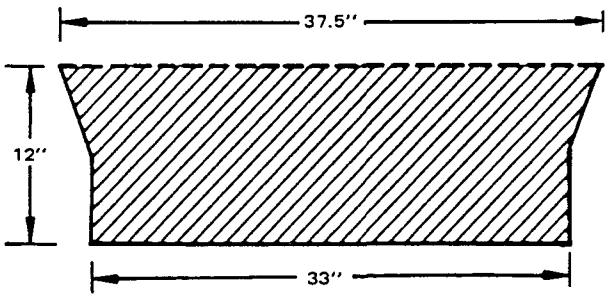

8C. RECESSED CANNISTER-TRIAD (RCT)

VISIBLE:
3 CYLINDRICAL CANNISTERS OF DIAMETER 10", LENGTH 48.75"

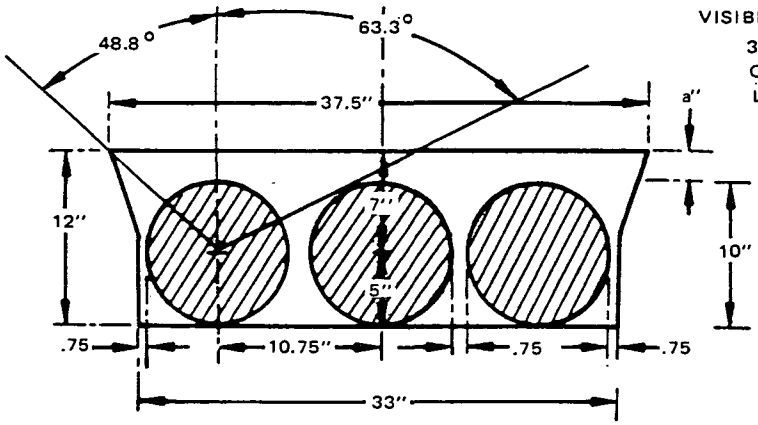

Figure 4-4. Tray Utilization Profiles

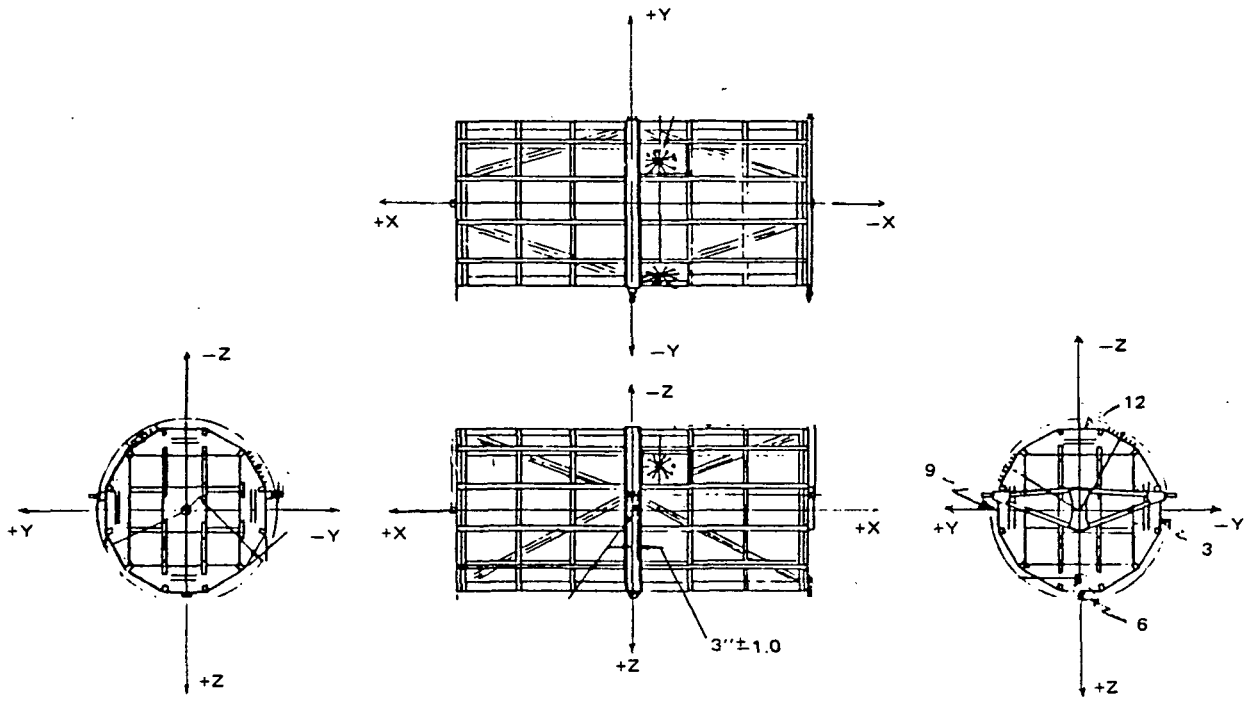

Figure 4-5. The LDEF Coordinate System

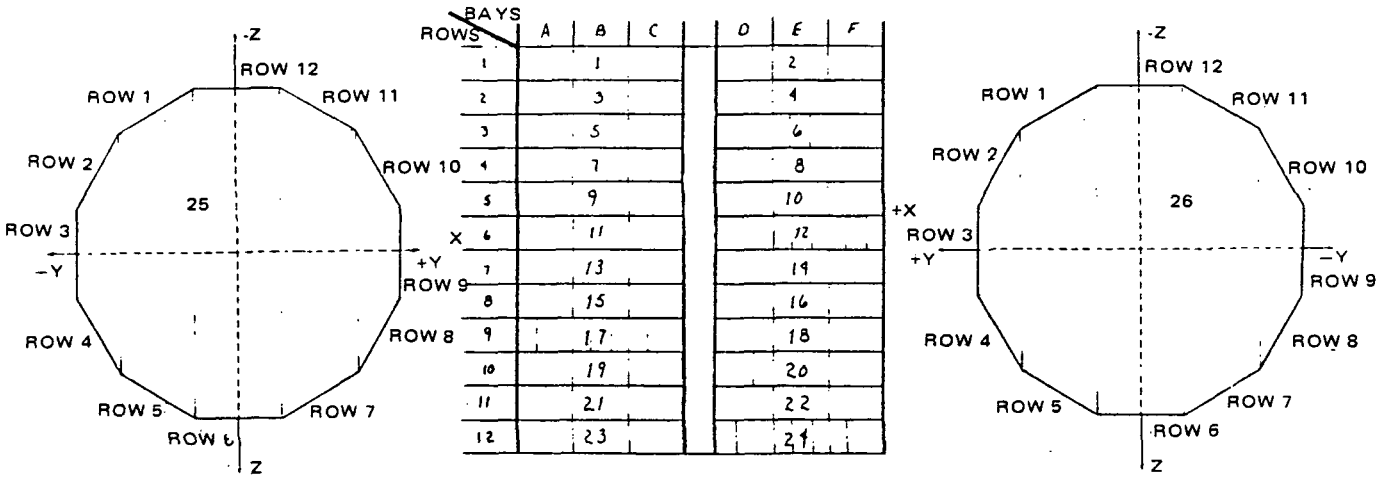

Figure 4-6. Definition of LDEF Rough-Surface Scattering Areas

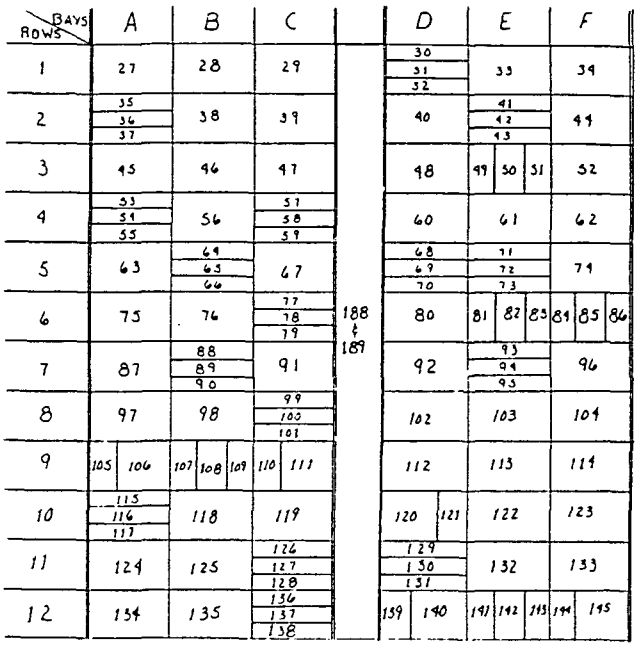

Figure 4-7. Identification of Simple Geometric Scatterers on LDEF Cylinder Surface

Figure 4-8. Identification of Simple Geometric Scatterers on LDEF H-Surface

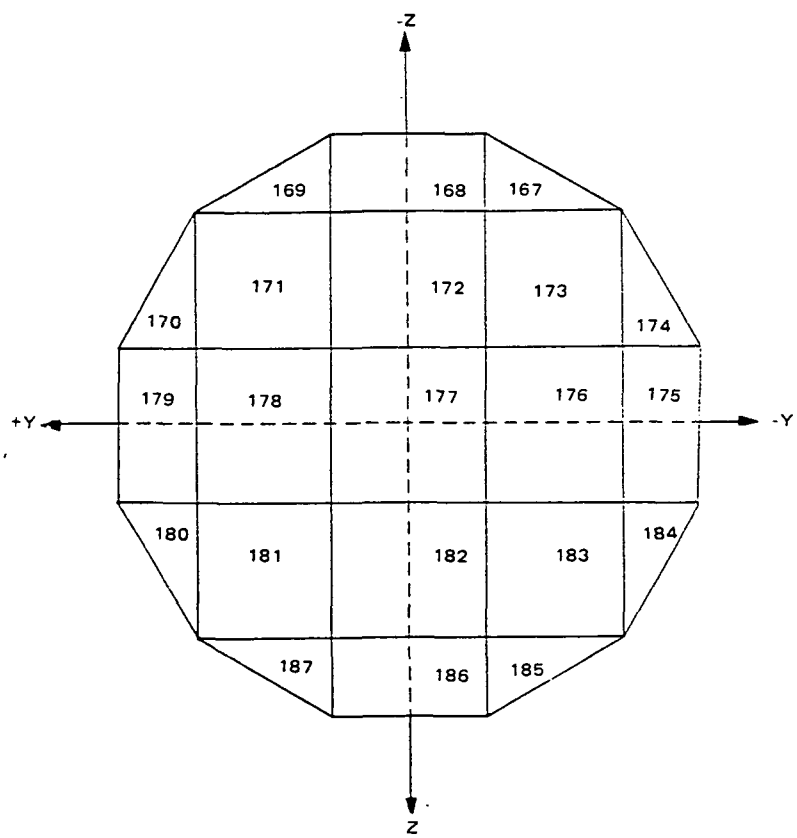

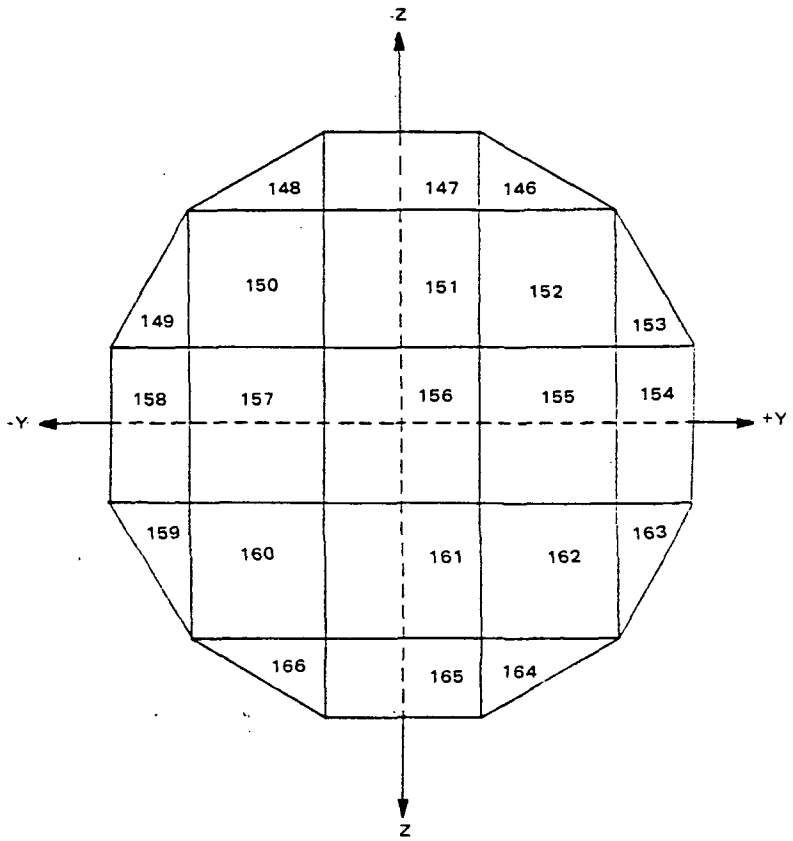

Figure 4-9. Identification of Simple Geometric Scatterers on LDEF G-Surface

TABLE 4-1. LDEF POINT TARGET CLASSIFICATION

Classification	Target Numbers
Rectangular, Rough Surface	1-26
Truncated Cylinder	30-32, 35-37, 41-43, 53-55, 57-59, 64-66, 68-70, 77-79, 88-90, 93-95, 99-101, 115-117, 126-131, 136-138, 188-189
Rectangular, Flat Plate	27-29, 33-34, 38-40, 44-52, 56, 60-63, 67, 74-76, 80-87, 91-92, 96-98, 102-114, 118-125, 132-135, 139-187

Using the classifications of Table 4-1 and the LDEF structural data, the point target parameters required for the computer model were generated and are summarized in Table 4-2. Computer code for the LDEF RCS model is documented in Appendix B of this report.

4.2.3 Solar Maximum Mission Spacecraft (SMMS) Model

Figure 4-10 gives a general illustration of SMMS, while Figure 4-11 gives an illustration of the coordinate system chosen for the SMMS. For this model, the x-axis is taken as coincident with the lengthwise axis of symmetry of the spacecraft with the origin being taken at the center of the transition adaptor. The TDRS parabolic dish antenna is along the minus-x axis and sun sensors are along the plus-x axis. The y-axis is defined so that it contains the points where the solar arrays connect to the transition adaptor. Plus-y protrudes from the transition adaptor on the side containing the shuttle grapple fixture. Scattering surfaces on SMMS are represented by 49 separate point targets. The first 19 targets are categorized as rough-surface scatterers and the surfaces they represent are depicted in Figure 4-12. Remaining scattering surfaces are approximated by simple geometric shapes. These surfaces are identified in Figure 4-13 and the geometric representations are summarized in Table 4-3. Note that the parabolic dish antenna was assumed to be in its nondeployed position. Finally, Table 4-4 summarizes the required point target parameter values determined from the surface classification identified above. Listing of the computer code is provided in Appendix B of this report.

4.2.4 Space Telescope Model

The Space Telescope satellite, shown in Figure 4-14, was originally modeled at NASA JSC as a large truncated cylinder concatenated with a smaller truncated cylinder. Results of theoretical RCS calculations using this model are provided in Figure 4-15. It was decided, however, that this model ignored many of the cultural features of the spacecraft. For example, the solar panels and data link antenna were ignored. Also, the large truncated cylinder is really not a smooth, round surface but is composed of 12 flat sides. Hence, the collection of point scatterers modeling approach seemed to be a natural for this spacecraft.

TABLE 4-2. LDEF POINT TARGET PARAMETERS

I	SIGMA	X	Y	Z	R	REGION OF NONZERO RCS			
						X-COMP	Y-COMP	Z-COMP	DEVIATION ANGLE
1	0.66	-2.23	1.04	-1.81	0.00	0.00000	0.50000	-0.86603	90.00
2	0.66	2.23	1.04	-1.81	0.00	0.00000	0.50000	-0.86603	90.00
3	0.66	-2.23	1.81	-1.04	0.00	0.00000	0.86603	-0.50000	90.00
4	0.66	2.23	1.81	-1.04	0.00	0.00000	0.86603	-0.50000	90.00
5	0.66	-2.23	2.09	0.00	0.00	0.00000	1.00000	0.00000	90.00
6	0.66	2.23	2.09	0.00	0.00	0.00000	1.00000	0.00000	90.00
7	0.66	-2.23	1.81	1.04	0.00	0.00000	0.86603	0.50000	90.00
8	0.66	2.23	1.81	1.04	0.00	0.00000	0.86603	0.50000	90.00
9	0.66	-2.23	1.04	1.81	0.00	0.00000	0.50000	0.86603	90.00
10	0.66	2.23	1.04	1.81	0.00	0.00000	0.50000	0.86603	90.00
11	0.66	-2.23	0.00	2.09	0.00	0.00000	0.00000	1.00000	90.00
12	0.66	2.23	0.00	2.09	0.00	0.00000	0.00000	1.00000	90.00
13	0.66	-2.23	-1.04	1.81	0.00	0.00000	-0.50000	0.86603	90.00
14	0.66	2.23	-1.04	1.81	0.00	0.00000	-0.50000	0.86603	90.00
15	0.66	-2.23	-1.81	1.04	0.00	0.00000	-0.86603	0.50000	90.00
16	0.66	2.23	-1.81	1.04	0.00	0.00000	-0.86603	0.50000	90.00
17	0.66	-2.23	-2.09	0.00	0.00	0.00000	-1.00000	0.00000	90.00
18	0.66	2.23	-2.09	0.00	0.00	0.00000	-1.00000	0.00000	90.00
19	0.66	-2.23	-1.81	-1.04	0.00	0.00000	-0.86603	-0.50000	90.00
20	0.66	2.23	-1.81	-1.04	0.00	0.00000	-0.86603	-0.50000	90.00
21	0.66	-2.23	-1.04	-1.81	0.00	0.00000	-0.50000	-0.86603	90.00
22	0.66	2.23	-1.04	-1.81	0.00	0.00000	-0.50000	-0.86603	90.00
23	0.66	-2.23	0.00	-2.09	0.00	0.00000	0.00000	-1.00000	90.00
24	0.66	2.23	0.00	-2.09	0.00	0.00000	0.00000	-1.00000	90.00
25	2.08	-4.57	0.00	0.00	0.00	-1.00000	0.00000	0.00000	90.00
26	2.08	4.57	0.00	0.00	0.00	1.00000	0.00000	0.00000	90.00
27	2800.00	-3.61	0.97	-1.68	0.00	0.00000	0.50000	-0.86603	1.50
28	2800.00	-2.23	1.04	-1.81	0.00	0.00000	0.50000	-0.86603	1.50
29	2800.00	-0.84	1.04	-1.81	0.00	0.00000	0.50000	-0.86603	1.50
						<PHIX<	<PHIY<	<PHIZ<	
30	56.60	0.84	0.72	-1.79	0.13	88.5 91.5	4.8 116.9	94.8 180.0	
31	56.60	0.84	0.96	-1.66	0.13	88.5 91.5	0.0 123.3	86.7 180.0	
32	56.60	0.84	1.19	-1.52	0.13	88.5 91.5	3.1 115.2	93.1 180.0	
						X-COMP	Y-COMP	Z-COMP	DEVIATION ANGLE
33	2800.00	2.23	1.04	-1.81	0.00	0.00000	0.50000	-0.86603	1.50
34	2800.00	3.61	1.04	-1.81	0.00	0.00000	0.50000	-0.86603	1.50
						<PHIX<	<PHIY<	<PHIZ<	
35	56.60	-3.61	1.52	-1.19	0.13	88.5 91.5	0.0 86.9	64.8 176.9	
36	56.60	-3.61	1.66	-0.96	0.13	88.5 91.5	0.0 93.3	56.7 180.0	
37	56.60	-3.61	1.79	-0.72	0.13	88.5 91.5	0.0 85.2	63.1 175.2	
						X-COMP	Y-COMP	Z-COMP	DEVIATION ANGLE
38	2800.00	-2.23	1.81	-1.04	0.00	0.00000	0.86603	-0.50000	1.50
39	2800.00	-0.84	1.81	-1.04	0.00	0.00000	0.86603	-0.50000	1.50
40	2800.00	0.84	1.81	-1.04	0.00	0.00000	0.86603	-0.50000	1.50
						<PHIX<	<PHIY<	<PHIZ<	
41	56.60	2.23	1.52	-1.19	0.13	88.5 91.5	0.0 86.9	64.8 176.9	
42	56.60	2.23	1.66	-0.96	0.13	88.5 91.5	0.0 93.3	56.7 180.0	
43	56.60	2.23	1.79	-0.72	0.13	88.5 91.5	0.0 85.2	63.1 175.2	

TABLE 4-2. LDEF POINT TARGET PARAMETERS (Continued)

I	SIGMA	X	Y	Z	R	REGION OF NONZERO RCS			
						X-COMP	Y-COMP	Z-COMP	DEVIATION ANGLE
44	2800.00	3.61	1.68	-0.97	0.00	0.00000	0.86603	-0.50000	1.50
45	2800.00	-3.61	2.09	0.00	0.00	0.00000	1.00000	0.00000	1.50
46	2800.00	-2.23	2.09	0.00	0.00	0.00000	1.00000	0.00000	1.50
47	2800.00	-0.84	2.09	0.00	0.00	0.00000	1.00000	0.00000	1.50
48	2800.00	0.84	2.09	0.00	0.00	0.00000	1.00000	0.00000	1.50
49	932.40	1.81	2.09	0.00	0.00	0.00000	1.00000	0.00000	1.50
50	2800.00	2.23	1.94	0.00	0.00	0.00000	1.00000	0.00000	1.50
51	932.40	1.81	2.09	0.00	0.00	0.00000	1.00000	0.00000	1.50
52	2800.00	3.61	2.09	0.00	0.00	0.00000	1.00000	0.00000	1.50
						<PHIX<	<PHIY<	<PHIZ<	
53	56.60	-3.61	1.79	0.72	0.13	88.5 91.5	0.0 85.2	4.8 116.9	
54	56.60	-3.61	1.66	0.96	0.13	88.5 91.5	0.0 93.3	0.0 123.3	
55	56.60	-3.61	1.52	1.19	0.13	88.5 91.5	0.0 86.9	3.1 115.2	
						X-COMP	Y-COMP	Z-COMP	DEVIATION ANGLE
56	2800.00	-2.23	1.81	1.04	0.00	0.00000	0.86603	0.50000	1.50
						<PHIX<	<PHIY<	<PHIZ<	
57	56.60	-0.84	1.79	0.72	0.13	88.5 91.5	0.0 85.2	4.8 116.9	
58	56.60	-0.84	1.66	0.96	0.13	88.5 91.5	0.0 93.3	0.0 123.3	
59	56.60	-0.84	1.52	1.19	0.13	88.5 91.5	0.0 86.9	3.1 115.2	
						X-COMP	Y-COMP	Z-COMP	DEVIATION ANGLE
0	2800.00	0.84	1.81	1.04	0.00	0.00000	0.86603	0.50000	1.50
61	2800.00	2.23	1.81	1.04	0.00	0.00000	0.86603	0.50000	1.50
62	2800.00	3.61	1.81	1.04	0.00	0.00000	0.86603	0.50000	1.50
63	2800.00	-3.61	1.04	1.81	0.00	0.00000	0.50000	0.86603	1.50
						<PHIX<	<PHIY<	<PHIZ<	
64	56.60	-2.23	1.19	1.52	0.13	88.5 91.5	3.1 115.2	0.0 86.9	
65	56.60	-2.23	0.96	1.66	0.13	88.5 91.5	0.0 123.3	0.0 93.3	
66	56.60	-2.23	0.72	1.79	0.13	88.5 91.5	4.8 116.9	0.0 85.2	
						X-COMP	Y-COMP	Z-COMP	DEVIATION ANGLE
67	2800.00	-0.84	1.04	1.81	0.00	0.00000	0.50000	0.86603	1.50
						<PHIX<	<PHIY<	<PHIZ<	
68	56.60	0.84	1.19	1.52	0.13	88.5 91.5	3.1 115.2	0.0 86.9	
69	56.60	0.84	0.96	1.66	0.13	88.5 91.5	0.0 123.3	0.0 93.3	
70	56.60	0.84	0.72	1.79	0.13	88.5 91.5	4.8 116.9	0.0 85.2	
71	56.60	2.23	1.19	1.52	0.13	88.5 91.5	3.1 115.2	0.0 86.9	
72	56.60	2.23	0.96	1.66	0.13	88.5 91.5	0.0 123.3	0.0 93.3	
73	56.60	2.23	0.72	1.79	0.13	88.5 91.5	4.8 116.9	0.0 85.2	
						X-COMP	Y-COMP	Z-COMP	DEVIATION ANGLE
74	2800.00	3.61	1.04	1.81	0.00	0.00000	0.50000	0.86603	1.50
75	2800.00	-3.61	0.00	2.09	0.00	0.00000	0.00000	1.00000	1.50
76	2800.00	-2.23	0.00	2.09	0.00	0.00000	0.00000	1.00000	1.50
						<PHIX<	<PHIY<	<PHIZ<	
77	56.60	-0.84	0.27	1.91	0.13	88.5 91.5	33.1 145.2	0.0 56.9	
78	56.60	-0.84	0.00	1.91	0.13	88.5 91.5	26.7 153.3	0.0 63.3	
79	56.60	-0.84	-0.27	1.91	0.13	88.5 91.5	34.8 144.9	0.0 56.9	

TABLE 4-2. LDEF POINT TARGET PARAMETERS (Continued)

I	SIGMA	X	Y	Z	R	REGION OF NONZERO RCS			
						X-COMP	Y-COMP	Z-COMP	DEVIATION ANGLE
80	2800.00	0.84	0.00	2.09	0.00	0.00000	0.00000	1.00000	1.50
81	932.40	1.81	0.00	2.09	0.00	0.00000	0.00000	1.00000	1.50
82	2800.00	2.23	0.00	1.94	0.00	0.00000	0.00000	1.00000	1.50
83	932.40	2.64	0.00	2.09	0.00	0.00000	0.00000	1.00000	1.50
84	932.40	3.20	0.00	2.09	0.00	0.00000	0.00000	1.00000	1.50
85	2800.00	3.61	0.00	1.94	0.00	0.00000	0.00000	1.00000	1.50
86	932.40	4.02	0.00	2.09	0.00	0.00000	0.00000	1.00000	1.50
87	2800.00	-3.61	-0.97	1.68	0.00	0.00000	-0.50000	0.86603	1.50
						<PHIX<	<PHIY<	<PHIZ<	
88	56.60	-2.23	-0.72	1.79	0.13	88.5 91.5	63.1 175.2	0.0 85.2	
89	56.60	-2.23	-0.96	1.66	0.13	88.5 91.5	56.7 180.0	0.0 93.3	
90	56.60	-2.23	-1.19	1.52	0.13	88.5 91.5	64.8 176.9	0.0 86.9	
						X-COMP	Y-COMP	Z-COMP	DEVIATION ANGLE
91	2800.00	-0.84	-1.04	1.81	0.00	0.00000	-0.50000	0.86603	1.50
92	2800.00	0.84	-1.04	1.81	0.00	0.00000	-0.50000	0.86603	1.50
						<PHIX<	<PHIY<	<PHIZ<	
93	56.60	2.23	-0.72	1.79	0.13	88.5 91.5	63.1 175.2	0.0 85.2	
94	56.60	2.23	-0.96	1.66	0.13	88.5 91.5	56.7 180.0	0.0 93.3	
95	56.60	2.23	-1.19	1.52	0.13	88.5 91.5	64.8 176.9	0.0 86.9	
						X-COMP	Y-COMP	Z-COMP	DEVIATION ANGLE
6	2800.00	3.61	-1.04	1.81	0.00	0.00000	-0.50000	0.86603	1.50
97	2800.00	-3.61	-1.81	1.04	0.00	0.00000	-0.86603	0.50000	1.50
98	2800.00	-2.23	-1.81	1.04	0.00	0.00000	-0.86603	0.50000	1.50
						<PHIX<	<PHIY<	<PHIZ<	
99	56.60	-0.84	-1.52	1.19	0.13	88.5 91.5	93.1 180.0	3.1 115.2	
100	56.60	-0.84	-1.66	0.96	0.13	88.5 91.5	86.7 180.0	0.0 123.3	
101	56.60	-0.84	-1.79	0.72	0.13	88.5 91.5	94.8 180.0	4.8 116.9	
						X-COMP	Y-COMP	Z-COMP	DEVIATION ANGLE
102	2800.00	0.84	-1.68	0.97	0.00	0.00000	-0.86603	0.50000	1.50
103	2800.00	2.23	-1.81	1.04	0.00	0.00000	-0.86603	0.50000	1.50
104	2800.00	3.61	-1.81	1.04	0.00	0.00000	-0.86603	0.50000	1.50
105	932.40	-4.02	-2.09	0.00	0.00	0.00000	-1.00000	0.00000	1.50
106	1867.60	-3.40	-1.94	0.00	0.00	0.00000	-1.00000	0.00000	1.50
107	932.40	-2.64	-2.09	0.00	0.00	0.00000	-1.00000	0.00000	1.50
108	2800.00	-2.23	-1.94	0.00	0.00	0.00000	-1.00000	0.00000	1.50
109	932.40	-1.81	-2.09	0.00	0.00	0.00000	-1.00000	0.00000	1.50
110	932.40	-1.25	-2.09	0.00	0.00	0.00000	-1.00000	0.00000	1.50
111	1867.60	-0.63	-1.94	0.00	0.00	0.00000	-1.00000	0.00000	1.50
112	2800.00	0.84	-2.09	0.00	0.00	0.00000	-1.00000	0.00000	1.50
113	2800.00	2.23	-2.09	0.00	0.00	0.00000	-1.00000	0.00000	1.50
114	2800.00	3.61	-2.09	0.00	0.00	0.00000	-1.00000	0.00000	1.50
						<PHIX<	<PHIY<	<PHIZ<	
115	56.60	-3.61	-1.79	-0.72	0.13	88.5 91.5	94.8 180.0	63.1 175.2	
116	56.60	-3.61	-1.66	-0.96	0.13	88.5 91.5	86.7 180.0	56.7 180.0	
117	56.60	-3.61	-1.52	-1.19	0.13	88.5 91.5	93.1 180.0	64.8 176.9	

TABLE 4-2. LDEF POINT TARGET PARAMETERS (Continued)

I	SIGMA	X	Y	Z	R	REGION OF NONZERO RCS			
						X-COMP	Y-COMP	Z-COMP	DEVIATION ANGLE
118	2800.00	-2.23	-1.81	-1.04	0.00	0.00000	-0.86603	-0.50000	1.50
119	2800.00	-0.84	-1.81	-1.04	0.00	0.00000	-0.86603	-0.50000	1.50
120	1867.60	0.63	-1.81	-1.04	0.00	0.00000	-0.86603	-0.50000	1.50
121	932.40	1.25	-1.81	-1.04	0.00	0.00000	-0.86603	-0.50000	1.50
122	2800.00	2.23	-1.81	-1.04	0.00	0.00000	-0.86603	-0.50000	1.50
123	2800.00	3.61	-1.81	-1.04	0.00	0.00000	-0.86603	-0.50000	1.50
124	2800.00	-3.61	-1.04	-1.81	0.00	0.00000	-0.50000	-0.86603	1.50
125	2800.00	-2.23	-1.04	-1.81	0.00	0.00000	-0.50000	-0.86603	1.50
						<PHIX<	<PHIY<	<PHIZ<	
126	56.60	-0.84	-1.19	-1.52	0.13	88.5 91.5	64.8 176.9	93.1 180.0	
127	56.60	-0.84	-0.96	-1.66	0.13	88.5 91.5	56.7 180.0	86.7 180.0	
128	56.60	-0.84	-0.72	-1.79	0.13	88.5 91.5	63.1 175.2	94.8 180.0	
129	56.60	0.84	-1.19	-1.52	0.13	88.5 91.5	64.8 176.9	93.1 180.0	
130	56.60	0.84	-0.96	-1.66	0.13	88.5 91.5	56.7 180.0	86.7 180.0	
131	56.60	0.84	-0.72	-1.79	0.13	88.5 91.5	63.1 175.2	94.8 180.0	
						X-COMP	Y-COMP	Z-COMP	DEVIATION ANGLE
132	2800.00	2.23	-1.04	-1.81	0.00	0.00000	-0.50000	-0.86603	1.50
133	2800.00	3.61	-1.04	-1.81	0.00	0.00000	-0.50000	-0.86603	1.50
134	2800.00	-3.61	0.00	-2.09	0.00	0.00000	0.00000	-1.00000	1.50
135	2800.00	-2.23	0.00	-2.09	0.00	0.00000	0.00000	-1.00000	1.50
						<PHIX<	<PHIY<	<PHIZ<	
136	56.60	-0.84	-0.27	-1.91	0.13	88.5 91.5	34.8 146.9	123.1 180.0	
137	56.60	-0.84	0.00	-1.91	0.13	88.5 91.5	26.7 153.3	116.7 180.0	
138	56.60	-0.84	0.27	-1.91	0.13	88.5 91.5	33.1 145.2	123.1 180.0	
						X-COMP	Y-COMP	Z-COMP	DEVIATION ANGLE
139	932.40	0.43	0.00	-2.09	0.00	0.00000	0.00000	-1.00000	1.50
140	1867.60	1.05	0.00	-2.09	0.00	0.00000	0.00000	-1.00000	1.50
141	932.40	2.64	0.00	-2.09	0.00	0.00000	0.00000	-1.00000	1.50
142	2800.00	2.23	0.00	-1.94	0.00	0.00000	0.00000	-1.00000	1.50
143	932.40	2.64	0.00	-2.09	0.00	0.00000	0.00000	-1.00000	1.50
144	932.40	3.20	0.00	-2.09	0.00	0.00000	0.00000	-1.00000	1.50
145	1867.60	3.82	0.00	-1.94	0.00	0.00000	0.00000	-1.00000	1.50
146	730.00	-4.57	1.04	-1.81	0.00	-1.00000	0.00000	0.00000	1.50
147	1694.00	-4.57	0.00	-1.81	0.00	-1.00000	0.00000	0.00000	1.50
148	730.00	-4.57	-1.04	-1.81	0.00	-1.00000	0.00000	0.00000	1.50
149	730.00	-4.57	-1.81	-1.04	0.00	-1.00000	0.00000	0.00000	1.50
150	2515.00	-4.42	-1.04	-1.04	0.00	-1.00000	0.00000	0.00000	1.50
151	2919.00	-4.42	0.00	-1.04	0.00	-1.00000	0.00000	0.00000	1.50
152	2515.00	-4.42	1.04	-1.04	0.00	-1.00000	0.00000	0.00000	1.50
153	730.00	-4.57	1.81	-1.04	0.00	-1.00000	0.00000	0.00000	1.50
154	1694.00	-4.57	1.81	0.00	0.00	-1.00000	0.00000	0.00000	1.50
155	2919.00	-4.57	1.04	0.00	0.00	-1.00000	0.00000	0.00000	1.50
156	3389.00	-4.57	0.00	0.00	0.00	-1.00000	0.00000	0.00000	1.50
157	2919.00	-4.57	-1.04	0.00	0.00	-1.00000	0.00000	0.00000	1.50
158	1694.00	-4.57	-1.81	0.00	0.00	-1.00000	0.00000	0.00000	1.50
159	730.00	-4.57	-1.81	1.04	0.00	-1.00000	0.00000	0.00000	1.50
160	2515.00	-4.57	-1.04	1.04	0.00	-1.00000	0.00000	0.00000	1.50
161	2919.00	-4.42	0.00	1.04	0.00	-1.00000	0.00000	0.00000	1.50
162	2515.00	-4.42	1.04	1.04	0.00	-1.00000	0.00000	0.00000	1.50

TABLE 4-2. LDEF POINT TARGET PARAMETERS (Continued)

I	SIGMA	X	Y	Z	R	REGION OF NONZERO RCS			
						X-COMP	Y-COMP	Z-COMP	DEVIATION ANGLE
163	730.00	-4.57	1.81	1.04	0.00	-1.00000	0.00000	0.00000	1.50
164	730.00	-4.57	1.04	1.81	0.00	-1.00000	0.00000	0.00000	1.50
165	1694.00	-4.57	0.00	1.81	0.00	-1.00000	0.00000	0.00000	1.50
166	730.00	-4.57	-1.04	1.81	0.00	-1.00000	0.00000	0.00000	1.50
167	730.00	4.57	-1.04	-1.81	0.00	1.00000	0.00000	0.00000	1.50
168	1694.00	4.57	0.00	-1.81	0.00	1.00000	0.00000	0.00000	1.50
169	730.00	4.57	1.04	-1.81	0.00	1.00000	0.00000	0.00000	1.50
170	730.00	4.57	1.81	-1.04	0.00	1.00000	0.00000	0.00000	1.50
171	2515.00	4.42	1.04	-1.04	0.00	1.00000	0.00000	0.00000	1.50
172	2919.00	4.57	0.00	-1.04	0.00	1.00000	0.00000	0.00000	1.50
173	2515.00	4.57	-1.04	-1.04	0.00	1.00000	0.00000	0.00000	1.50
174	730.00	4.57	-1.81	-1.04	0.00	1.00000	0.00000	0.00000	1.50
175	1694.00	4.57	-1.81	0.00	0.00	1.00000	0.00000	0.00000	1.50
176	2919.00	4.42	-1.04	0.00	0.00	1.00000	0.00000	0.00000	1.50
177	3389.00	4.57	0.00	0.00	0.00	1.00000	0.00000	0.00000	1.50
178	2919.00	4.42	1.04	0.00	0.00	1.00000	0.00000	0.00000	1.50
179	1694.00	4.57	1.81	0.00	0.00	1.00000	0.00000	0.00000	1.50
180	730.00	4.57	1.81	1.04	0.00	1.00000	0.00000	0.00000	1.50
181	2515.00	4.57	1.04	1.04	0.00	1.00000	0.00000	0.00000	1.50
182	2919.00	4.42	0.00	1.04	0.00	1.00000	0.00000	0.00000	1.50
183	2515.00	4.57	-1.04	1.04	0.00	1.00000	0.00000	0.00000	1.50
184	730.00	4.57	-0.18	1.04	0.00	1.00000	0.00000	0.00000	1.50
185	730.00	4.57	-1.04	1.81	0.00	1.00000	0.00000	0.00000	1.50
16	1694.00	4.57	0.00	1.81	0.00	1.00000	0.00000	0.00000	1.50
37	730.00	4.57	1.04	1.81	0.00	1.00000	0.00000	0.00000	1.50
						<PHIX<	<PHIY<	<PHIZ<	
188	3.48	0.00	0.00	0.00	2.06	88.5 91.5	0.0 90.0	0.0 180.0	
189	3.48	0.00	0.00	0.00	2.06	88.5 91.5	90.0 180.0	0.0 180.0	

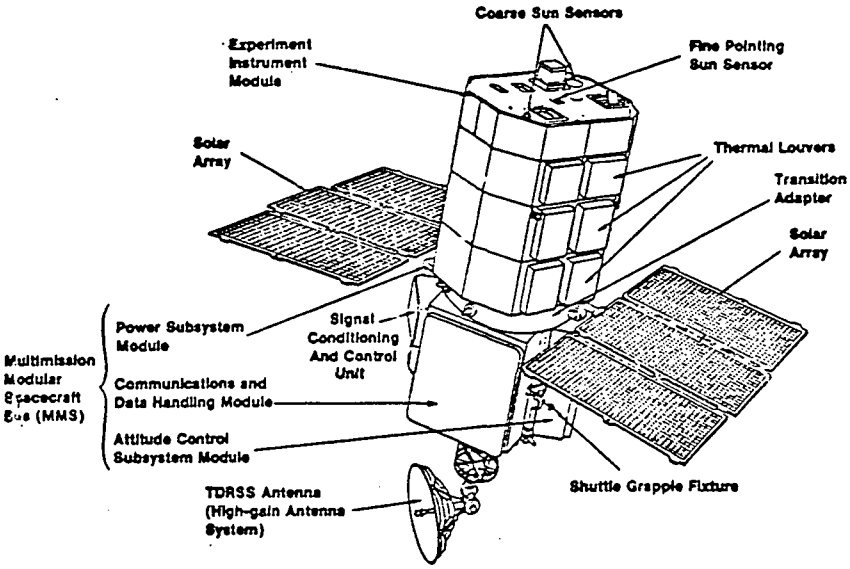

Figure 4-10. SMM Spacecraft

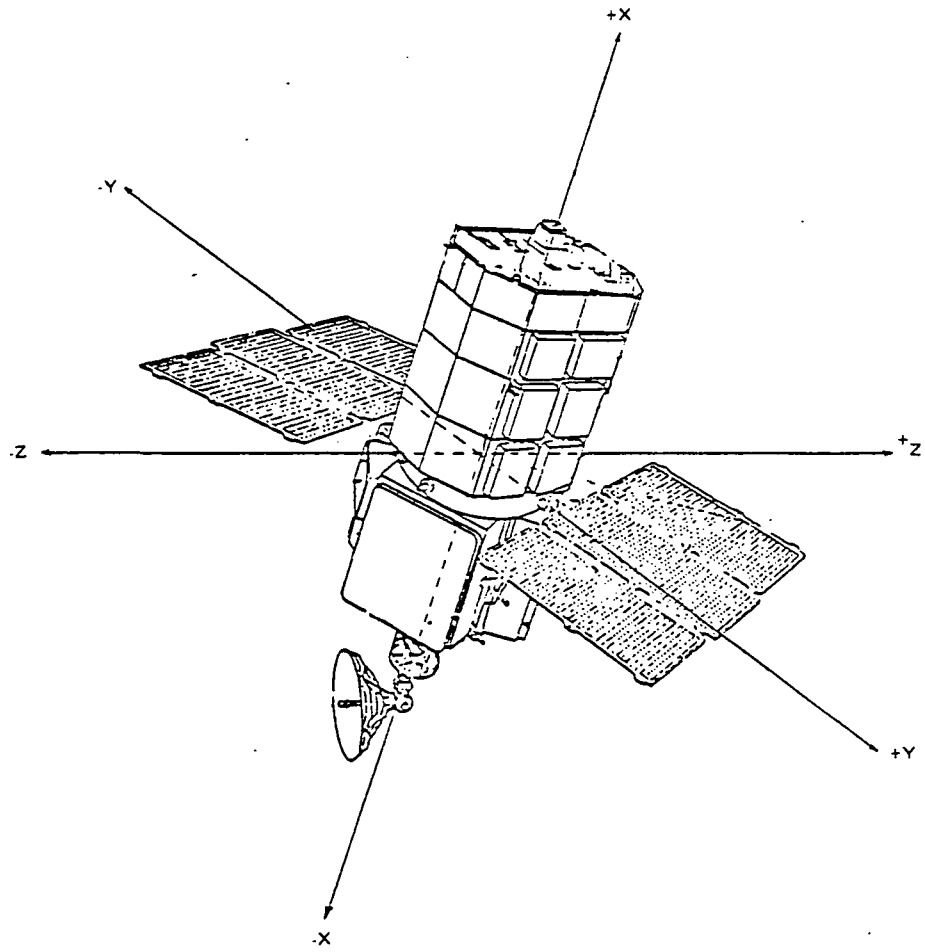

Figure 4-11. SMMS Coordinate System

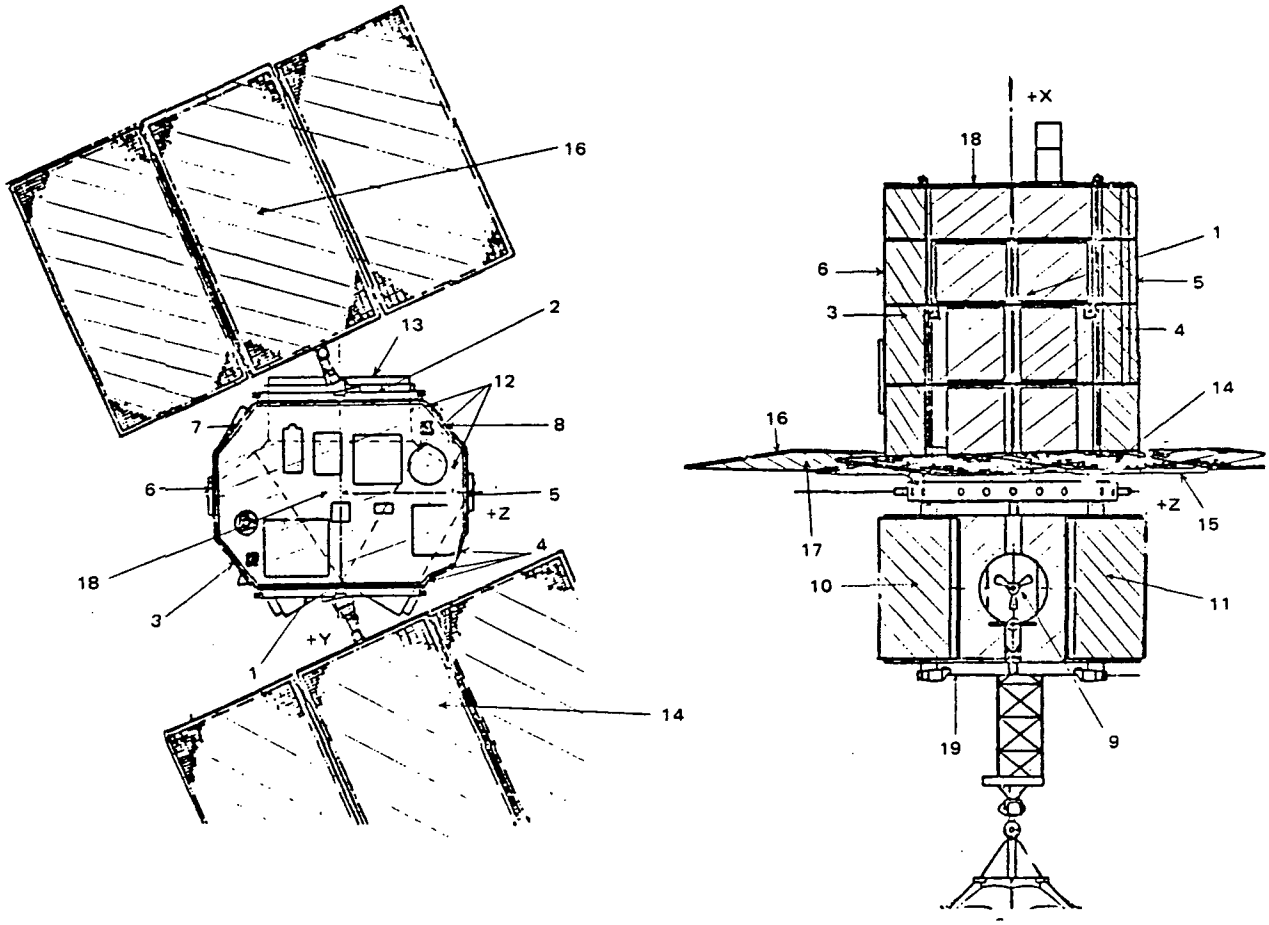

Figure 4-12. Definition of SMMS Rough-Surface Scattering Areas

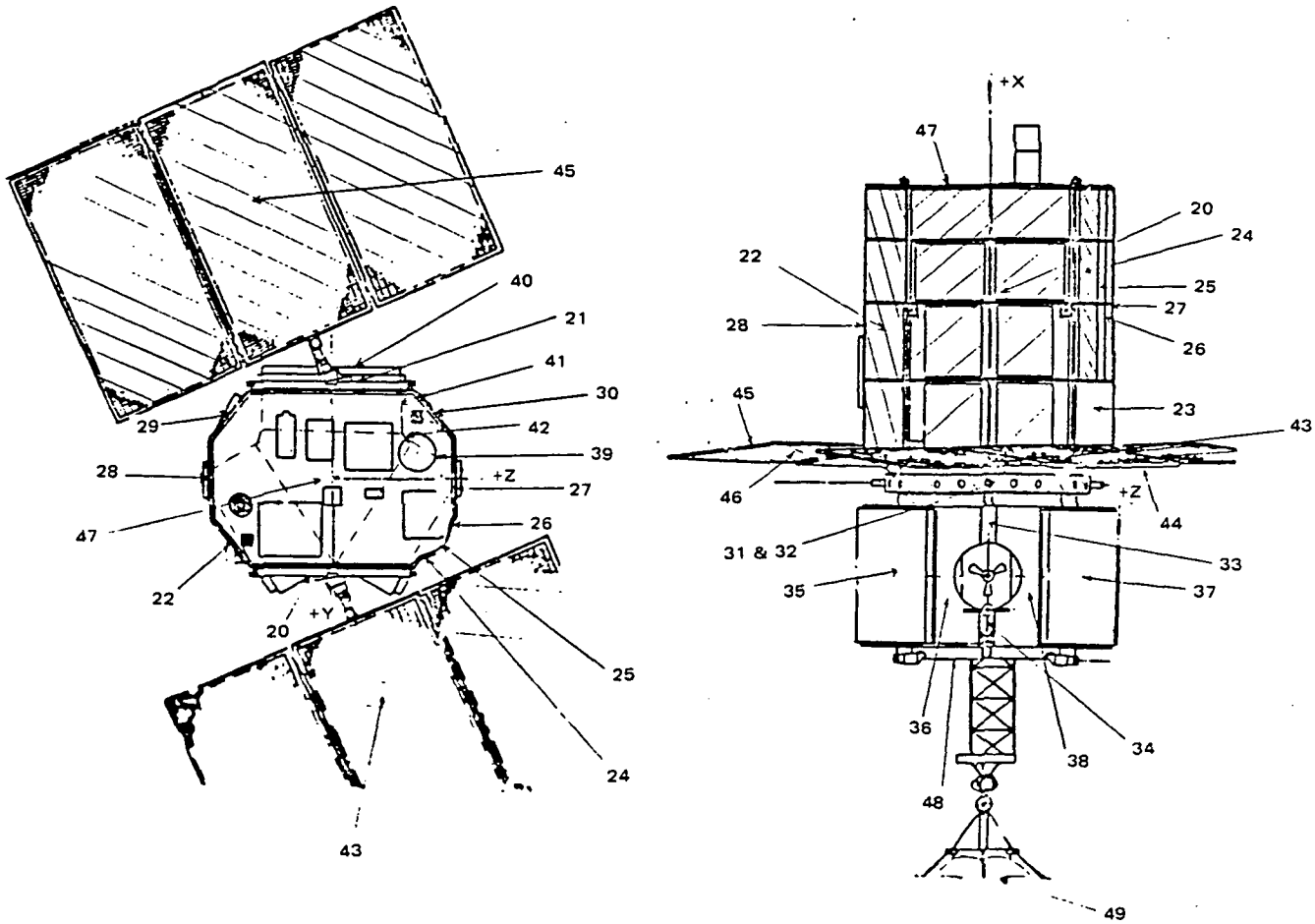

Figure 4-13. Identification of Simple Geometric Scatterers on SMMS

TABLE 4-3. SMMS POINT TARGET CLASSIFICATION

Classification	Target Numbers
Rectangular, Rough-Surface	1-19
Rectangular, Flat Plates	20-30, 33-46
Truncated Cylinder	31, 32
Parabolic Dish Antenna	49
Circular, Flat Plates	47, 48

TABLE 4-4. SMMS POINT SCATTERER PARAMETERS

I	SIGMA	X	Y	Z	R	REGION OF NONZERO RCS			
						X-COMP	Y-COMP	Z-COMP	DEVIATION ANGLE
1	0.10	1.39	0.86	0.00	0.00	0.00000	1.00000	0.00000	90.00
2	0.10	1.39	-0.86	0.00	0.00	0.00000	-1.00000	0.00000	90.00
3	0.02	1.39	0.56	-0.93	0.00	0.00000	0.64280	-0.76600	90.00
4	0.02	1.39	0.56	0.93	0.00	0.00000	0.64280	0.76600	90.00
5	0.03	1.39	0.00	1.06	0.00	0.00000	0.00000	1.00000	90.00
6	0.03	1.39	0.00	-1.06	0.00	0.00000	0.00000	-1.00000	90.00
7	0.01	1.39	0.56	-0.88	0.00	0.00000	-0.64940	-0.76040	90.00
8	0.01	1.39	0.56	0.88	0.00	0.00000	-0.63610	0.77160	90.00
9	0.01	1.39	0.75	0.00	0.00	0.00000	1.00000	0.00000	90.00
10	0.02	-0.77	0.44	-0.77	0.00	0.00000	0.49240	-0.87040	90.00
11	0.02	-0.77	1.10	0.85	0.00	0.00000	0.87040	0.49240	90.00
12	0.01	-0.77	-0.36	0.64	0.00	0.00000	0.64280	0.76600	90.00
13	0.02	-0.77	-0.95	0.00	0.00	0.00000	-1.00000	0.00000	90.00
14	0.70	0.27	2.23	0.62	0.00	0.99760	0.06370	0.02840	90.00
15	0.70	0.23	2.23	0.62	0.00	-0.99760	-0.06370	-0.02840	90.00
16	0.70	0.27	-2.23	-0.62	0.00	0.99760	-0.06370	-0.02840	90.00
17	0.70	0.23	-2.23	-0.62	0.00	-0.99760	0.06370	0.02840	90.00
18	0.06	2.49	0.00	0.00	0.00	1.00000	0.00000	0.00000	90.00
19	0.06	-1.50	0.00	0.00	0.00	-1.00000	0.00000	0.00000	90.00
20	2419.00	1.39	0.83	0.00	0.00	0.00000	1.00000	0.00000	1.50
21	2419.00	1.39	-0.83	0.00	0.00	0.00000	-1.00000	0.00000	1.50
22	373.00	1.39	0.56	-0.93	0.00	0.00000	0.64280	-0.76600	1.50
23	7.25	0.54	0.56	0.93	0.00	0.00000	0.64280	0.76600	1.50
24	21.84	1.63	0.66	0.83	0.00	0.00000	0.92720	0.37460	1.50
25	11.14	1.63	0.57	0.93	0.00	0.00000	0.51500	0.85720	1.50
26	18.83	1.63	0.44	0.99	0.00	0.00000	0.29240	0.95630	1.50
27	663.00	1.39	0.00	1.06	0.00	0.00000	0.00000	1.00000	1.50
28	663.00	1.39	0.00	-1.06	0.00	0.00000	0.00000	-1.00000	1.50
29	321.00	1.39	0.56	-0.88	0.00	0.00000	-0.64940	-0.76040	1.50
30	321.00	1.39	0.56	0.88	0.00	0.00000	-0.63610	0.77160	1.50
						<PHIX<	<PHIY<	<PHIZ<	
31	3.63	0.00	0.00	0.00	0.75	89.2 90.8	0.0 90.0	0.0 180.0	
32	3.63	0.00	0.00	0.00	0.80	89.2 90.8	90.0 180.0	0.0 180.0	
						X-COMP	Y-COMP	Z-COMP	DEVIATION ANGLE
33	0.92	-0.41	0.75	0.00	0.00	0.00000	1.00000	0.00000	1.50
34	0.97	-1.15	0.75	0.00	0.00	0.00000	1.00000	0.00000	1.50
35	470.00	-0.77	0.44	-0.77	0.00	0.00000	0.49240	-0.87040	1.50
36	82.13	-0.77	0.87	-0.26	0.00	0.00000	0.87040	0.49240	1.50
37	470.00	-0.77	1.10	0.85	0.00	0.00000	0.49240	0.87040	1.50
38	83.00	-0.77	0.87	0.27	0.00	0.00000	0.86600	-0.50000	1.50
39	83.00	-0.77	-0.21	0.90	0.00	0.00000	-0.86600	0.50000	1.50
40	470.00	-0.77	-0.95	0.00	0.00	0.00000	-1.00000	0.00000	1.50
41	83.00	-0.77	-0.68	0.58	0.00	0.00000	0.00000	1.00000	1.50
42	6.34	-0.77	-0.36	0.64	0.00	0.00000	-0.64280	0.76600	1.50
43	16995.00	0.27	2.23	0.62	0.00	0.99760	0.06370	0.02840	1.50
44	16995.00	0.23	2.23	0.62	0.00	-0.99760	-0.06370	-0.02840	1.50
45	16995.00	0.27	-2.23	-0.62	0.00	0.99760	-0.06370	-0.02840	1.50
46	16995.00	0.23	-2.23	-0.62	0.00	-0.99760	0.06370	0.02840	1.50
47	146615.00	2.49	0.00	0.00	0.00	1.00000	0.00000	0.00000	1.50
48	146615.00	-1.50	0.00	0.00	0.00	-1.00000	0.00000	0.00000	1.50
						<PHIX<	<PHIY<	<PHIZ<	
49	0.33	-1.50	0.00	0.00	0.65	178.5 180.0	88.5 91.5	88.5 91.5	

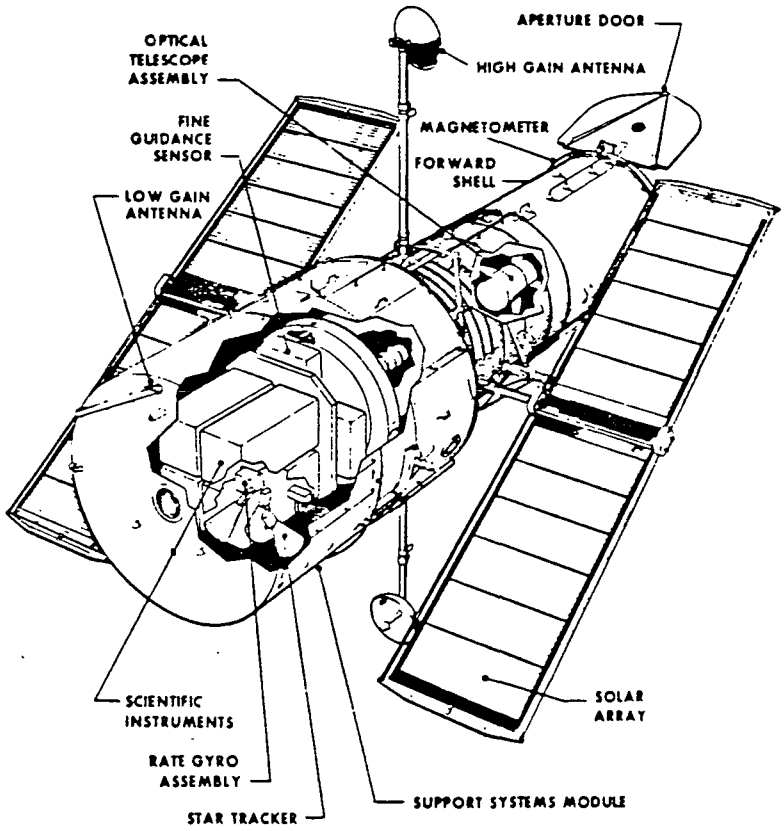

Figure 4-14. Space Telescope Spacecraft

Figure 4-15. RCS as Function of Aspect Angle for Two Concatenated Cylinder Model Shown Above

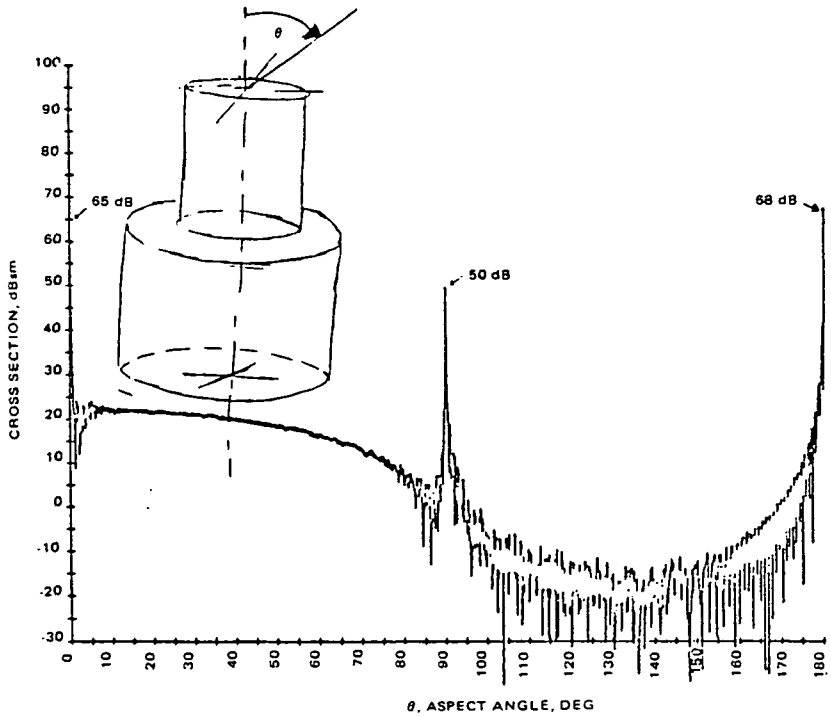

In fact, two RCS computer models were developed for this spacecraft. One model assumes the solar panels and data link antennas are stowed and the aperture door is closed. This model will be referred to as the stowed model in the sequel. In the second model, denoted as the deployed model, the solar panels and antennas are deployed and the aperture door is open.

Stowed Model Description. Figures 4-16 and 4-17 illustrate the placement of the coordinate system for the Space Telescope. This coordinate system is the same for the deployed version as well. The x-axis is taken as coincident with the axis of the two cylinders. Placement of the origin is at the interface of the two cylinders with minus-x on the small cylinder side. The y-axis is defined so that the x-y plane contains the two stowed dish antennas. Positive-y direction can be distinguished by noting that the aperture door hinge has a positive y coordinate.

Following the modeling procedure outlined above, the next step is to identify the rough-surface scatterers and the surfaces that can be represented by simple-geometric objects. Figure 4-16 identifies all of the surfaces represented by the rough-surface scattering model and Figure 4-17 identifies all surfaces represented by simple-geometric shapes.

Construction of the Space Telescope model has one additional modeling feature not found in the standard procedure. This feature addresses the problem of modeling the scattering off the interface where the two cylinders are joined. Theoretical predictions of Figure 4-15 show the right angle nature of this interface produces significant cross section values over a large range of aspect angles (0 to 80 degrees). This contribution, while predicted from a simple model, cannot be ignored. However, at the same time, it is very hard to model this effect with a single point or a group of points. Therefore, a compromise was made which utilizes both modeling techniques. The interface is represented by a point located on the x-axis at the interface. Cross section contributions from this point are computed in the following way. First, the angle between the x-axis and the unit vector toward the radar is computed using

$$\theta = \cos^{-1}\left(-u_R\,(1)\right) \qquad (4\text{-}2)$$

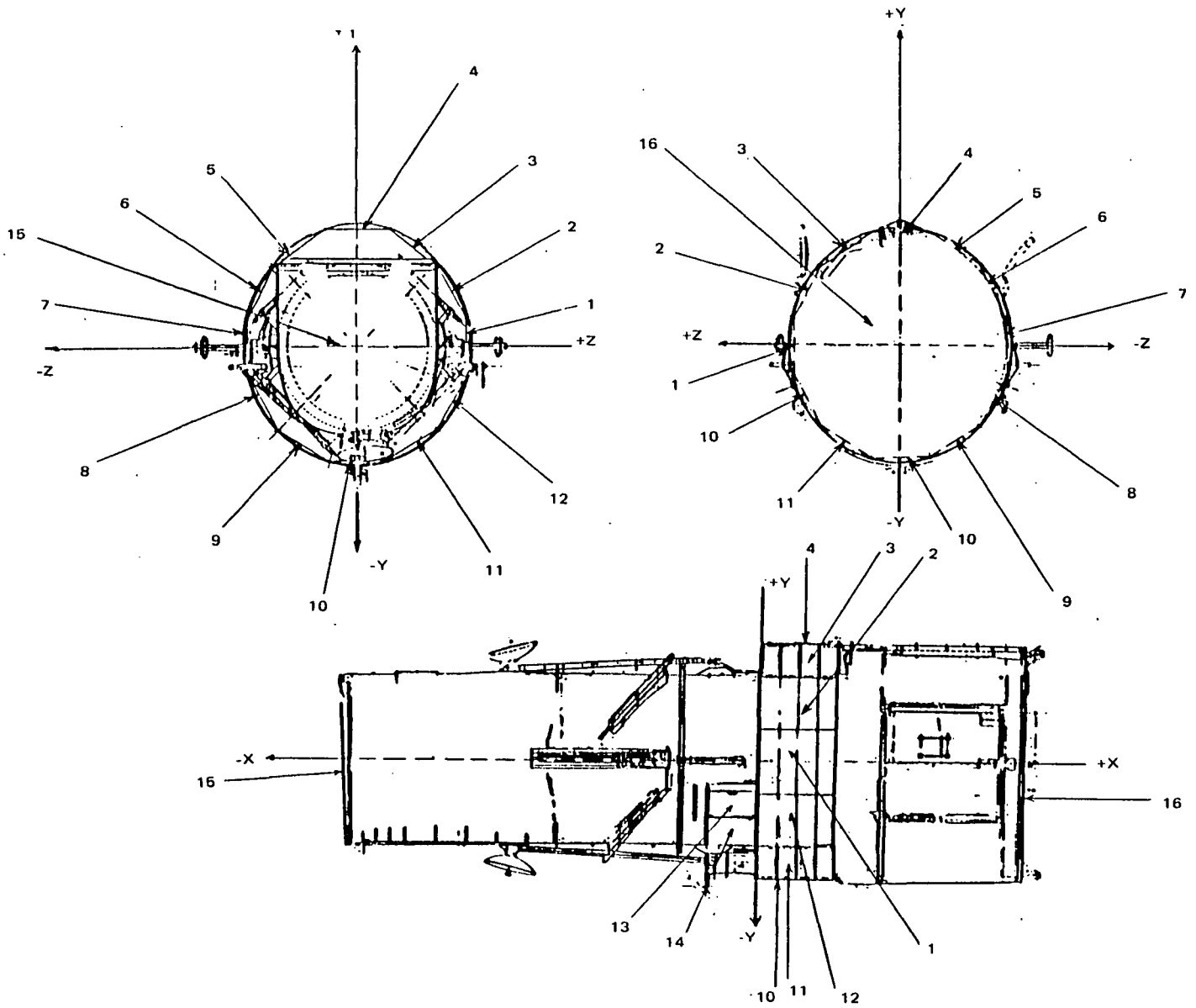

Figure 4-16. Definition of Rough-Surface Scattering Areas for Stowed Version of Space Telescope

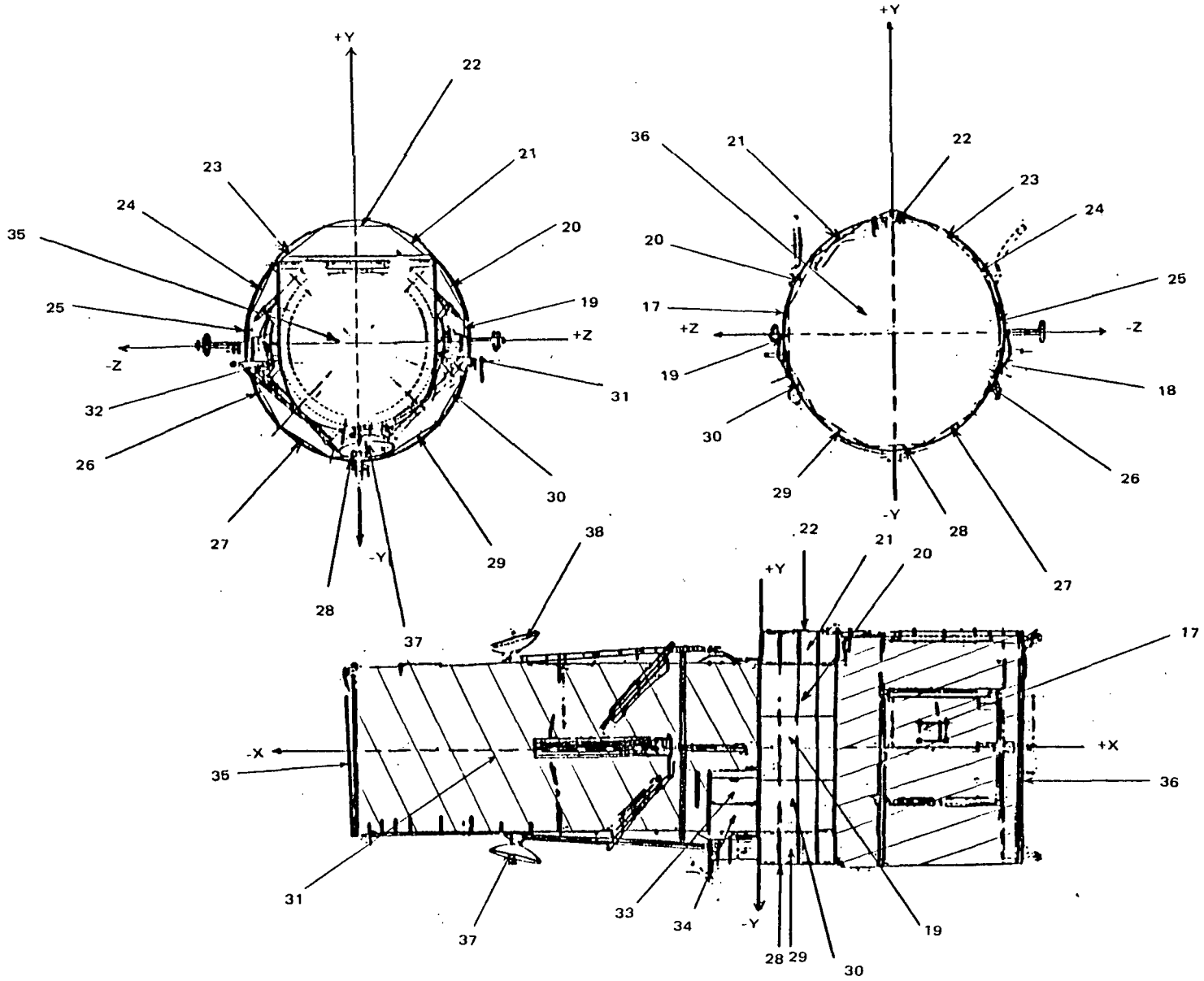

Figure 4-17. Identification of Simple-Geometric Scatterers on Stowed Version of Space Telescope

where $u_R(1)$ is the x-component of the unit vector in the direction of the radar. This angle is then used to compute the cross section contribution from the interface using the functional form shown in Figure 4-18. This functional form represents a simplified model of the "sidelobe" region of the theoretical results given in Figure 4-15. In addition, this cross section value is randomized to reflect the fine structure shown in Figure 4-15.

Table 4-5 provides the classification of the entire set of points comprising the model. Table 4-6 summarizes the required point target parameter values determined from the surface classifications identified in Table 4-5.

Deployed Model Description. The deployed model contains all of the scatterers defined for the stowed model with the addition of point targets for the solar panels and the inside of the aperture door. Surfaces represented as rough-surface scatterers are identified in Figure 4-19 and surfaces represented by simple-geometric scattering models are illustrated in Figure 4-20. Table 4-7 provides a summary of target classifications and Table 4-8 gives a summary of the point target parameter values required for the computer model.

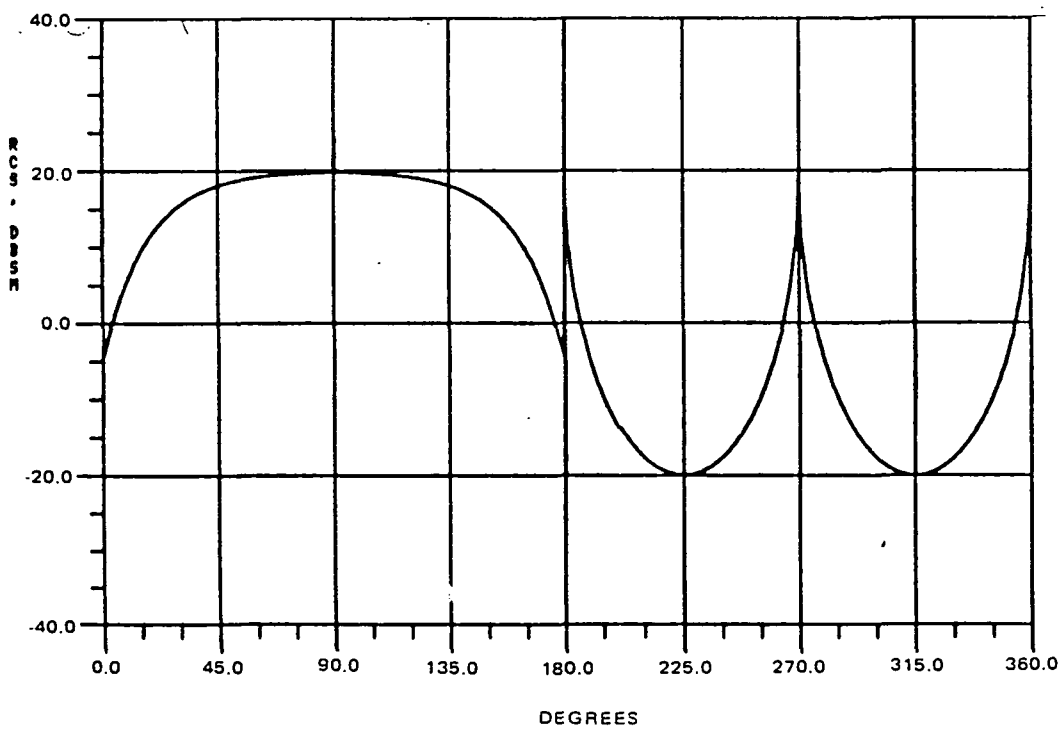

Figure 4-18. Radar Cross Section Amplitude Function for Special Point Target Model

TABLE 4-5. SPACE TELESCOPE (STOWED) POINT TARGET CLASSIFICATION

Classification	Target Number
Rectangular, Rough Surface	1-16
Rectangular, Flat Plate	19-30, 33, 34
Circular Flat Plate	35, 36
Truncated Cylinder	17, 18, 31, 32
Parabolic Dish Antenna	37, 38
Special Interface Model	39, 40

TABLE 4-6. SPACE TELESCOPE STOWED VERSION POINT TARGET PARAMETERS

I	SIGMA	X	Y	Z	R	REGION OF NONZERO RCS			
						X-COMP	Y-COMP	Z-COMP	DEVIATION ANGLE
1	0.02	0.78	0.00	2.06	0.00	0.00000	0.00000	1.00000	90.00
2	0.02	0.78	1.03	1.78	0.00	0.00000	0.50000	0.86600	90.00
3	0.02	0.78	1.78	1.03	0.00	0.00000	0.86600	0.50000	90.00
4	0.02	0.78	2.06	0.00	0.00	0.00000	1.00000	0.00000	90.00
5	0.02	0.78	1.78	-1.03	0.00	0.00000	0.86600	-0.50000	90.00
6	0.02	0.78	1.03	-1.78	0.00	0.00000	0.50000	-0.86600	90.00
7	0.02	0.78	0.00	-2.06	0.00	0.00000	0.00000	-1.00000	90.00
8	0.02	0.78	-1.03	-1.78	0.00	0.00000	-0.50000	-0.86600	90.00
9	0.02	0.78	-1.78	-1.03	0.00	0.00000	-0.86600	-0.50000	90.00
10	0.02	0.78	-2.06	0.00	0.00	0.00000	-1.00000	0.00000	90.00
11	0.02	0.78	-1.78	1.03	0.00	0.00000	-0.86600	0.50000	90.00
12	0.02	0.78	-1.03	1.78	0.00	0.00000	-0.50000	0.86600	90.00
13	0.01	-0.48	-0.70	1.47	0.00	0.00000	-0.42260	0.90630	90.00
14	0.01	-0.48	-1.28	1.02	0.00	0.00000	-0.86600	0.50000	90.00
15	0.97	-8.09	0.00	0.00	0.00	0.06980	-0.06980	0.00000	90.00
16	2.27	5.35	0.00	0.00	0.00	1.00000	0.00000	0.00000	90.00
						<PHIX<	<PHIY<	<PHIZ<	
17	1525.60	3.31	0.00	0.00	2.13	89.2 90.8	0.0 90.0	0.0 180.0	
18	1525.60	3.31	0.00	0.00	2.13	89.2 90.8	90.0 180.0	0.0 180.0	
						X-COMP	Y-COMP	Z-COMP	DEVIATION ANGLE
19	9230.00	0.78	0.00	2.06	0.00	0.00000	0.00000	1.00000	1.50
20	9230.00	0.78	1.03	1.78	0.00	0.00000	0.50000	0.86600	1.50
21	9230.00	0.78	1.78	1.03	0.00	0.00000	0.86600	0.50000	1.50
22	9230.00	0.78	2.06	0.00	0.00	0.00000	1.00000	0.00000	1.50
23	9230.00	0.78	1.78	-1.03	0.00	0.00000	0.86600	-0.50000	1.50
24	9230.00	0.78	1.03	-1.78	0.00	0.00000	0.50000	-0.86600	1.50
25	9230.00	0.78	0.00	-2.06	0.00	0.00000	0.00000	-1.00000	1.50
26	9230.00	0.78	-1.03	-1.78	0.00	0.00000	-0.50000	-0.86600	1.50
27	9230.00	0.78	-1.78	-1.03	0.00	0.00000	-0.86600	-0.50000	1.50
28	9230.00	0.78	-2.06	0.00	0.00	0.00000	-1.00000	0.00000	1.50
29	9230.00	0.78	-1.78	1.03	0.00	0.00000	-0.86600	0.50000	1.50
30	9230.00	0.78	-1.03	1.78	0.00	0.00000	-0.50000	0.86600	1.50
						<PHIX<	<PHIY<	<PHIZ<	
31	5268.00	-4.14	0.00	0.00	1.47	89.2 90.8	0.0 90.0	0.0 180.0	
32	5268.00	-4.14	0.00	0.00	1.47	89.2 90.8	90.0 180.0	0.0 180.0	
						X-COMP	Y-COMP	Z-COMP	DEVIATION ANGLE
33	3423.00	-0.48	-0.70	1.47	0.00	0.00000	-0.42260	0.90630	1.50
34	2917.00	-0.48	-1.28	1.02	0.00	0.00000	-0.86600	0.50000	1.50
35	20000.00	-8.09	0.00	0.00	0.00	-0.99760	-0.06980	0.00000	1.50
36	20000.00	5.35	0.00	0.00	0.00	1.00000	0.00000	0.00000	1.50
37	1079.00	-4.97	-2.23	0.00	0.00	-0.22500	-0.97440	0.00000	1.50
38	1079.00	-4.97	2.23	0.00	0.00	-0.22500	0.97440	0.00000	1.50
						<PHIX<	<PHIY<	<PHIZ<	
39	0.00	0.00	0.00	0.00	1.80	0.0 180.0	0.0 180.0	0.0 90.0	
40	0.00	0.00	0.00	0.00	1.80	0.0 180.0	0.0 180.0	90.0 180.0	

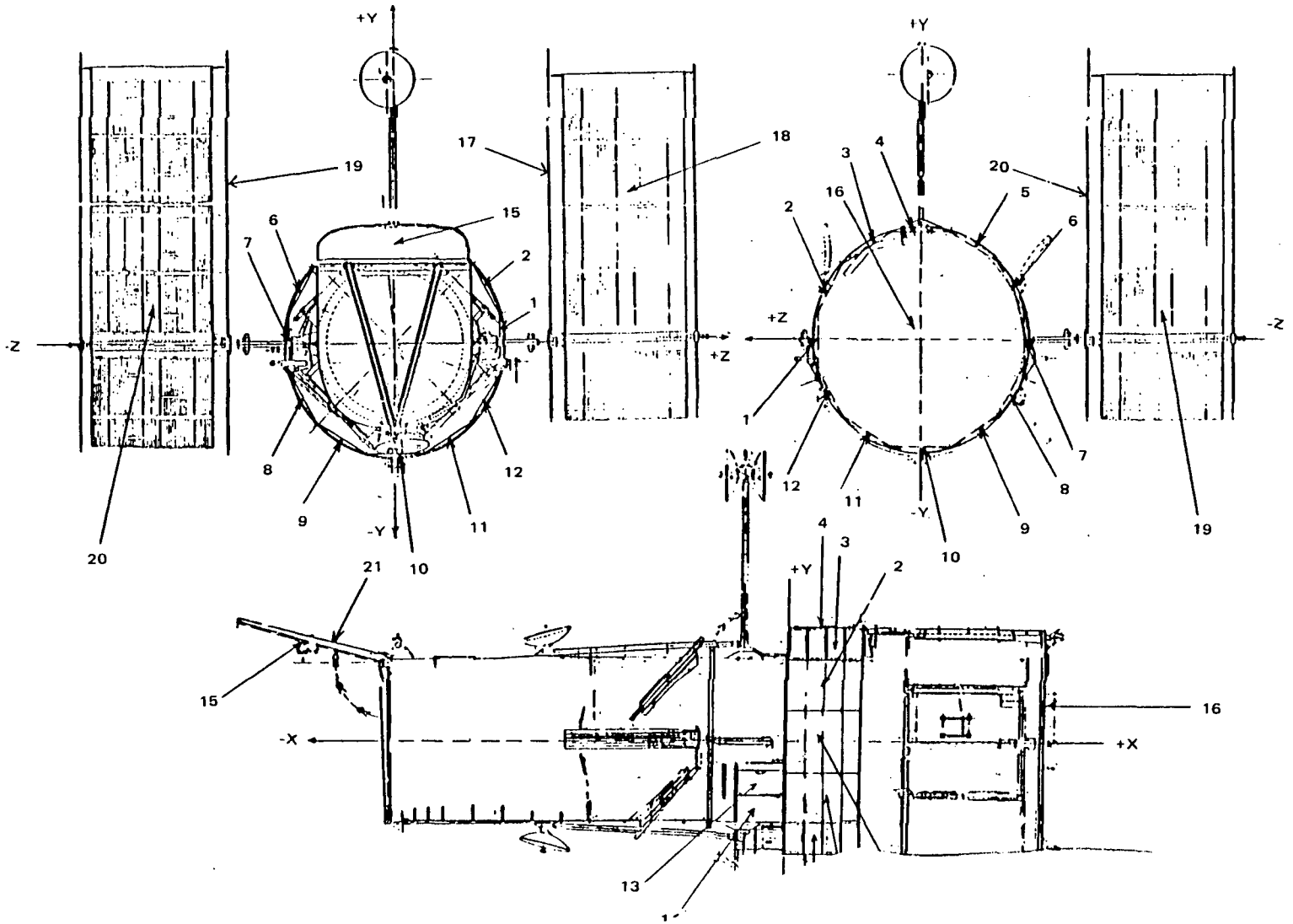

Figure 4-19. Definition of Rough-Surface Scattering Areas for Deployed Version of Space Telescope

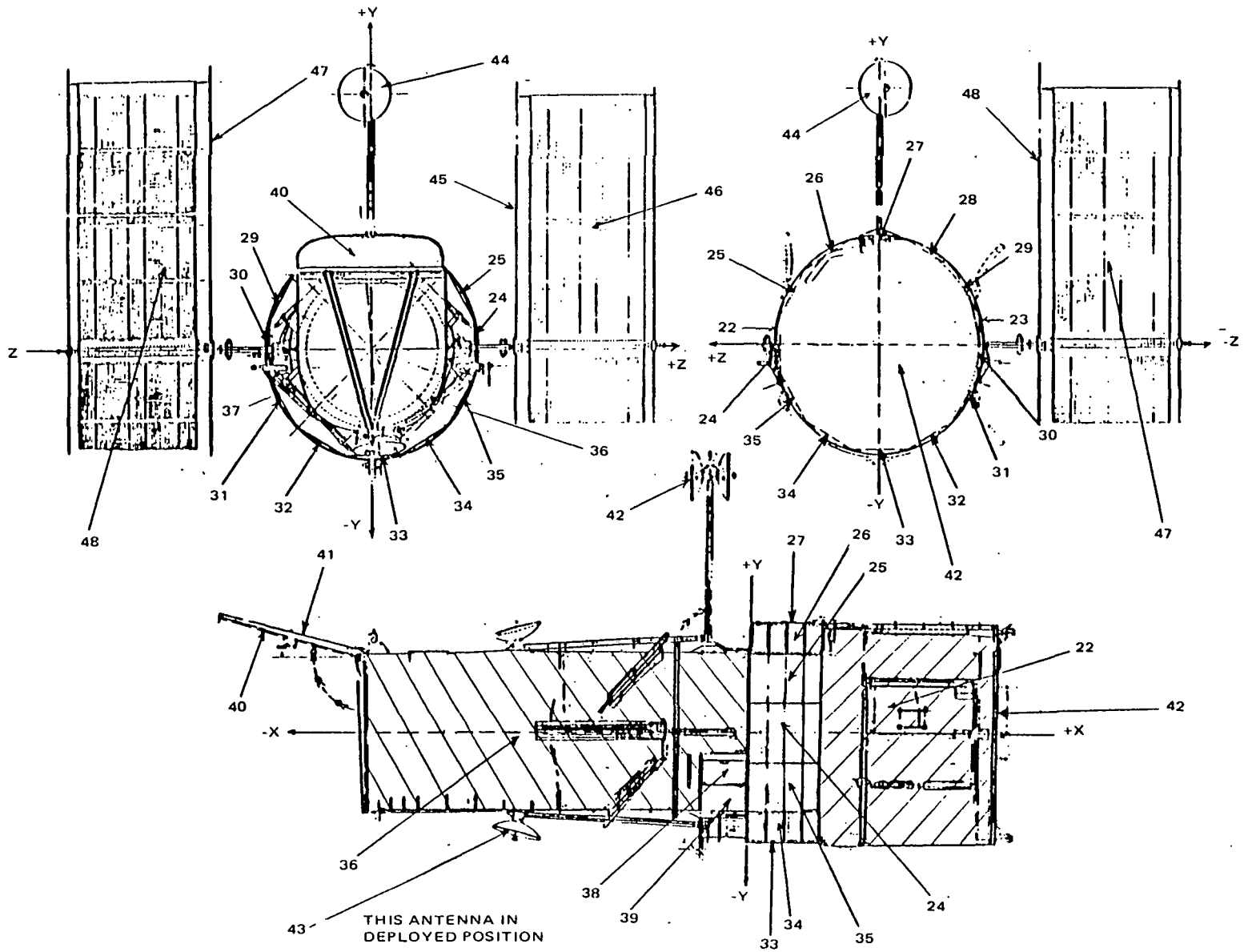

Figure 4-20. Identification of Simple-Geometric Scatterers on Delayed Version of Space Telescope

TABLE 4-7. SPACE TELESCOPE (DEPLOYED) POINT TARGET CLASSIFICATION

Classification	Target Number
Rectangular, Rough-Surface	1-21
Rectangular, Flat Plate	24-35, 38-41, 45-48
Circular, Flat Plage	42
Truncated Cylinders	22, 23, 36, 37
Parabolic Dish Antenna	43, 44
Special Interface Model	49, 50

TABLE 4-8. SPACE TELESCOPE DEPLOYED VERSION POINT TARGET PARAMETERS

I	SIGMA	X	Y	Z	R	REGION OF NONZERO RCS			
						X-COMP	Y-COMP	Z-COMP	DEVIATION ANGLE
1	0.02	0.78	0.00	2.06	0.00	0.00000	0.00000	1.00000	90.00
2	0.02	0.78	1.03	1.78	0.00	0.00000	0.50000	0.86600	90.00
3	0.02	0.78	1.78	1.03	0.00	0.00000	0.86600	0.50000	90.00
4	0.02	0.78	2.06	0.00	0.00	0.00000	1.00000	0.00000	90.00
5	0.02	0.78	1.78	-1.03	0.00	0.00000	0.86600	-0.50000	90.00
6	0.02	0.78	1.03	-1.78	0.00	0.00000	0.50000	-0.86600	90.00
7	0.02	0.78	0.00	-2.06	0.00	0.00000	0.00000	-1.00000	90.00
8	0.02	0.78	-1.03	-1.78	0.00	0.00000	-0.50000	-0.86600	90.00
9	0.02	0.78	-1.78	-1.03	0.00	0.00000	-0.86600	-0.50000	90.00
10	0.02	0.78	-2.06	0.00	0.00	0.00000	-1.00000	0.00000	90.00
11	0.02	0.78	-1.78	1.03	0.00	0.00000	-0.86600	0.50000	90.00
12	0.02	0.78	-1.03	1.78	0.00	0.00000	-0.50000	0.86600	90.00
13	0.01	-0.48	-0.70	1.47	0.00	0.00000	-0.42260	0.90630	90.00
14	0.01	-0.48	-1.28	1.02	0.00	0.00000	-0.86600	0.50000	90.00
15	0.97	-9.33	1.99	0.00	0.00	-0.06980	-0.99760	0.00000	90.00
16	2.27	5.35	0.00	0.00	0.00	1.00000	0.00000	0.00000	90.00
17	7.13	-0.26	0.00	4.78	0.00	1.00000	0.00000	0.00000	90.00
18	7.13	-0.26	0.00	4.78	0.00	-1.00000	0.00000	0.00000	90.00
19	7.13	-0.26	0.00	-4.78	0.00	1.00000	0.00000	0.00000	90.00
20	7.13	-0.26	0.00	-4.78	0.00	-1.00000	0.00000	0.00000	90.00
21	0.97	-9.33	1.99	0.00	0.00	0.23770	0.97130	0.00000	90.00
						<PHIX<	<PHIY<	<PHIZ<	
22	1525.60	3.31	0.00	0.00	2.13	88.5 91.5	0.0 90.0	0.0 180.0	
23	1525.60	3.31	0.00	0.00	2.13	88.5 91.5	90.0 180.0	0.0 180.0	
						X-COMP	Y-COMP	Z-COMP	DEVIATION ANGLE
24	9230.00	0.78	0.00	2.06	0.00	0.00000	0.00000	1.00000	1.50
25	9230.00	0.78	1.03	1.78	0.00	0.00000	0.50000	0.86600	1.50
26	9230.00	0.78	1.78	1.03	0.00	0.00000	0.86600	0.50000	1.50
27	9230.00	0.78	2.06	0.00	0.00	0.00000	1.00000	0.00000	1.50
28	9230.00	0.78	1.78	-1.03	0.00	0.00000	0.86600	-0.50000	1.50
29	9230.00	0.78	1.03	-1.78	0.00	0.00000	0.50000	-0.86600	1.50
30	9230.00	0.78	0.00	-2.06	0.00	0.00000	0.00000	-1.00000	1.50
31	9230.00	0.78	-1.03	-1.78	0.00	0.00000	-0.50000	-0.86600	1.50
32	9230.00	0.78	-1.78	-1.03	0.00	0.00000	-0.86600	-0.50000	1.50
33	9230.00	0.78	-2.06	0.00	0.00	0.00000	-1.00000	0.00000	1.50
34	9230.00	0.78	-1.78	1.03	0.00	0.00000	-0.86600	0.50000	1.50
35	9230.00	0.78	-1.03	1.78	0.00	0.00000	-0.50000	0.86600	1.50
						<PHIX<	<PHIY<	<PHIZ<	
36	5268.00	-4.14	0.00	0.00	1.47	88.5 91.5	0.0 90.0	0.0 180.0	
37	5268.00	-4.14	0.00	0.00	1.47	88.5 91.5	90.0 180.0	0.0 180.0	
						X-COMP	Y-COMP	Z-COMP	DEVIATION ANGLE
38	3423.00	-0.48	-0.70	1.47	0.00	0.00000	-0.42260	0.90630	1.50
39	2917.00	-0.48	-1.28	1.02	0.00	0.00000	-0.86600	0.50000	1.50
40	20000.00	-9.33	1.99	0.00	0.00	-0.06980	-0.99760	0.00000	1.50
41	20000.00	-9.33	1.99	0.00	0.00	0.23770	0.97130	0.00000	1.50
42	20000.00	5.35	0.00	0.00	0.00	1.00000	0.00000	0.00000	1.50
43	1079.00	-1.40	-5.16	-0.51	0.00	-1.00000	0.00000	0.00000	1.50
44	1079.00	-1.40	5.16	-0.51	0.00	-1.00000	0.00000	0.00000	1.50
45	20000.00	-0.26	0.00	4.78	0.00	1.00000	0.00000	0.00000	1.50
46	20000.00	-0.26	0.00	4.78	0.00	-1.00000	0.00000	0.00000	1.50
47	20000.00	-0.26	0.00	-4.78	0.00	1.00000	0.00000	0.00000	1.50
48	20000.00	-0.26	0.00	-4.78	0.00	-1.00000	0.00000	0.00000	1.50
						<PHIX<	<PHIY<	<PHIZ<	
49	0.00	0.00	0.00	0.00	1.80	0.0 180.0	0.0 180.0	0.0 90.0	
50	0.00	0.00	0.00	0.00	1.80	0.0 180.0	0.0 180.0	90.0 180.0	

5. REFERENCES

1. "Ku-Band Rendezvous Radar Performance Computer Simulation Model Final Report," Hughes Aircraft Company, July 1980.

2. G.A. Young, "Ku-Band System Signature Log," Reference HS237-4514, Hughes Aircraft Company, January 1984.

3. R.S. Austin, "Failure to Break Track Anomaly Observed During Radar Tests at KSC," Internal AVO to C.L. Mohler, 13 January 1984.

4. P.J. Holzer, "Description and Accuracy Assessment of Radar Signal Strength Indicator in Space Shuttle Orbits," IDC HS237-4044, 22 April 1982.

5. "Ku-Band Integrated Radar and Communications Subsystem Preliminary Design Review, Volume III Electronics Assembly 2," Reference HS237-1531-3, Hughes Aircraft Company, March 1978.

6. "Ku-Band Radar Acquisition Study GPC ACQ Mode Final Report," Hughes Reference No. D9771 SCG830444R, 31 July 1983.

7. Development Specification Radar/Communications Electronic Assembly, Part 2 for the Ku-Band Integrated Radar and Communications Equipment, Revision C," Hughes Aircraft Company, 10 March 1982.

APPENDIX A. DERIVATION OF USEFUL EXPRESSIONS FOR AGC UPDATE AND RSS

The purpose of this appendix is to provide derivations of useful expressions for two important quantities, AGC update (AGCERR) and RSS. These two parameters can be expressed in terms of the signal-to-thermal noise power ratio at the doppler filter output SNR_{DT}, the unAGC'd system thermal noise power level, and the precomputed AGC threshold. The noise power level and the AGC threshold are well-known design values. Hence, the expressions derived herein will relate AGC update and RSS to SNR_{DT} and will be extremely useful in evaluating system operation.

A.1 DERIVATION OF AGC UPDATE EXPRESSION

A simplified mathematical model, shown in Figure A-1, is used as the basis of the derivation. The signal is assumed to be the appropriate pulse train at some general doppler frequency with unAGC'd power S. Thermal noise is assumed to be additive with unAGC'd power N_T. A/D quantization noise is assumed to be additive with power N_Q ($= q^2/12$), while all other quantization noise sources are ignored. Digital processing of the signal plus noise terms consists of the following stages. First, the signal plus noise is passed through a coherent integrator of gain G. This stage essentially represents the range gating, presumming, and doppler filtering processes. Next, the signal plus noise is magnitude detected, and its mean level computed. Finally, this mean level is converted to a logarithmic value (in dB) and the AGC update term (in dB) is then computed by differencing this mean level with the precomputed threshold given in log form.

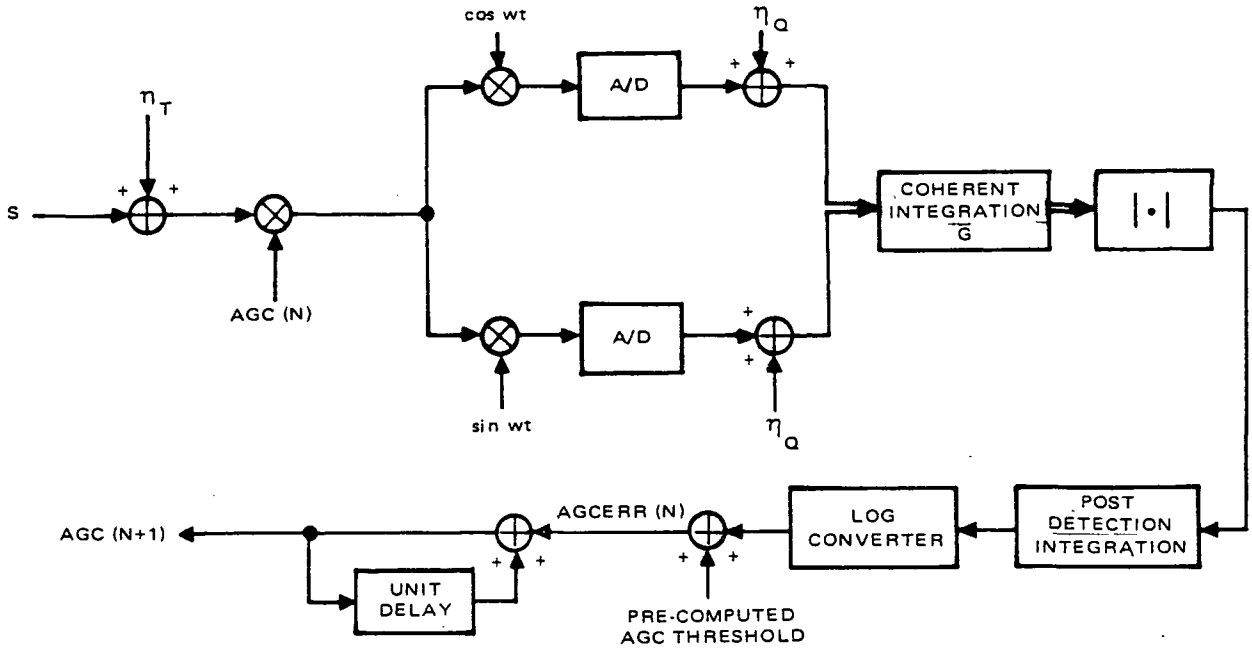

Figure A-1. Simplified Mathematical Model Used to Derive Useful Expressions for AGC Update and RSS

Derivation of the expression for the AGC update begins by writing the total signal-plus-noise power at the A/D output. That is,

$$\text{Total Signal Plus Noise Power @ A/D Output} = AGC(N)\,(S+N_T) + N_Q \qquad \text{(A-1)}$$

After coherent integration and magnitude detection, the total signal-plus-noise power becomes

$$\text{Total Signal Plus Noise Power @ Detector Output} = P_T = AGC(N)\,(G^2S + GN_T) + GN_Q \qquad \text{(A-2)}$$

Finally, the AGC update, i.e., the required change in the AGC for the next data cycle is given by

$$AGCERR(N) = K - 10\ \text{Log}\ (P_T) \qquad \text{(A-3)}$$

where K is interpreted as the "desired" power level at the log converter output and 10 log (P_T) is interpreted as the "actual" power level at the log converter output.

The next task is to develop a useful expression for K. Its development is based upon the fact that the purpose of the AGC is to maintain the steady-state signal-plus-noise power level at the A/D input to $(2q)^2$ where q represents the height of a single A/D step. A major assumption which was made when computing the design values for K was that the signal power S was much greater than the thermal noise power, N_T, at the A/D input for all tracking situations of interest. Hence, the thermal noise power could be ignored and the signal power, S, could be taken as $4q^2$. Another assumption in the determination of K was to observe that $4q^2 >> q^2/12$ and, hence, the quantization noise power contribution at the A/D output could be ignored. Results of these two assumptions can be summarized as follows.

$$\text{Desired Power Level at A/D output} = 4q^2 = S \qquad \text{(A-4)}$$

Results of coherent integration, magnitude detection, and log conversion produce the following design equation for K,

$$K = 10 \log (G^2 S) = 10 \log (G^2\ 4q^2) \qquad \text{(A-5)}$$

Now, combining Equations A-2, A-3, and A-5, we obtain

$$AGCERR(N) = 10 \log (G^2\ 4q^2) - 10 \log (AGC(N)(G^2 S + GN_T) + GN_Q)$$

or, converting AGCERR(N) to a power ratio,

$$AGCERR(N) = \frac{4q^2\ G^2}{AGC(N)(G^2 S + GN_T) + GN_Q}$$

or

$$AGCERR(N) = \frac{(4q^2/N_T)\ G}{AGC(N)(SNR_{DT} + 1) + N_Q/N_T}$$

N_T has a design value of $(2.8q)^2$ in the low sample rate mode and a value of $(12.5q)^2$ in the high sample rate mode. (Remember that N_T is the unAGC'd thermal noise power at the A/D input.) N_Q is assumed to have a value of $q^2/12$ and the values for G are pulsewidth and PRF dependent as shown in Table 2-1 of the text.

A.2 DERIVATION OF RSS EXPRESSION

From the text we know that the RSS can be expressed in terms of AGC as follows:

$$RSS(N) = 10 \log (1/AGC(N)) + AGC(0) \qquad (A-7)$$

where AGC(0) is approximately -6 dB. We now seek to replace AGC(N) with quantities that provide more insight into system operation. To this end, we make the following assumption. It is assumed that the system AGC has reached steady state, i.e., AGC(N) = AGC(N+1) or, equivalently, AGCERR(N) = 1. From Equation A-6 this implies

$$1/AGC(N) = (SNR_{DT} + 1)(N_T/(4q^2 G - N_Q))$$

Noting that $4q^2G >> N_Q = q^2/12$ and that $SNR_{DT} = G\ SNR_{VT}$, we can now rewrite the above equation in the form

$$RSS(N) = 10 \log (SNR_{VT} + 1/G) + 10 \log (N_T/4q^2) + AGC(0) \qquad (A-8)$$

Simplifying the expression further, it can easily be shown that $SNR_{VT} >> 1/G$ for all nonnegative RSS values and also notice that $10 \log (N_T/4q^2) + AGC(0)$ is a constant, C_s, for a given sample rate. Therefore, Equation A-8 can be rewritten

$$RSS(N) = SNR_{VT}\ (dB) + C_s \qquad (A-9)$$

This was the desired result.

There are some observations that can be made about the RSS expressed in this form. First, one might predict a discontinuity in RSS at the sample rate change (2560 feet closing and 3200 feet opening in passive mode) because there is a discontinuity in SNR_{VT} at this point. However, there is no discontinuity in RSS because the change in C_s at the sample rate transition exactly compensates for the discontinuity in SNR_{VT}.

The second observation is that it would also be useful to have RSS as a function of target range and target radar cross section. Equation A-9 can be converted to this form using either the low sample rate SNR_{VT} and C_s or the high sample rate SNR_{VT} and C_s. The result is

$$RSS(N) = 185.6 - 40 \log R + 10 \log RCS - 3.1 \qquad \text{(A-10)}$$

where

R = target range in feet,
RCS = target radar cross section in square meters.

APPENDIX B. COMPUTER PROGRAM LISTINGS

Appendix B is furnished only in selected volumes due to its size. Any person having a need for the information contained in this appendix can obtain a copy by contacting H. G. Magnusson, Building R1, M/S B211, El Segundo, telephone number (213) 648-9170.